INTERNATIONAL JOURNAL FOR NUMERICAL METHODS IN FLUIDS
Int. J. Numer. Meth. Fluids 2004 **45**:1047–1082 (DOI: 10.1002/fld.729)

Zero mass error using unsteady wetting–drying conditions in shallow flows over dry irregular topography

P. Brufau[1,†], P. García-Navarro[1,*,‡] and M. E. Vázquez-Cendón[2,¶]

[1]*Fluid Mechanics, Centro Politécnico Superior, University of Zaragoza, María de Luna, Edif. Torres Quevedo, 50018 Zaragoza, Spain*
[2]*Applied Mathematics, University of Santiago de Compostela, Spain*

SUMMARY

A wetting–drying condition (WDC) for unsteady shallow water flow in two dimensions leading to zero numerical error in mass conservation is presented in this work. Some applications are shown which demonstrate the effectiveness of the WDC in flood propagation and dam break flows over real geometries. The WDC has been incorporated into a cell centred finite volume method based on Roe's approximate Riemann solver across the edges of both structured and unstructured meshes. Previous wetting–drying condition based on steady-state conditions lead to numerical errors in unsteady cases over configurations with strong variations on bed slope. A modification of the wetting–drying condition including the normal velocity to the cell edge enables to achieve zero numerical errors. The complete numerical technique is described in this work including source terms discretization as a complete and efficient 2D river flow simulation tool. Comparisons of experimental and numerical results are shown for some of the applications. Copyright © 2004 John Wiley & Sons, Ltd.

KEY WORDS: wetting/drying; unsteady shallow flows; complex topography; numerical modelling

1. INTRODUCTION

Many engineering and environmental problems involve the study of water flows. Free surface flow includes large scale motion of water in rivers which is characterized by the presence of a free surface and by a vertical scale much smaller than the horizontal one, hence commonly modelled as shallow water flows. River flows are mostly unsteady and can be described by the shallow water model [1] which form a set of non-linear hyperbolic equations. A great amount of literature exists describing 1D and 2D numerical models and various computational techniques using finite difference, finite element and finite volume methods to obtain the satisfactory solution of unsteady river flow problems [2–4].

*Correspondence to: P. García-Navarro, Fluid Mechanics, Centro Politécnico Superior, University of Zaragoza, María de Luna, Edif. Torres Quevedo, 50018 Zaragoza, Spain.
†E-mail: brufau@unizar.es
‡E-mail: pigar@unizar.es
¶E-mail: malenav@usc.es

Published online 4 May 2004

Received 29 March 2003
Revised 7 March 2004

The accurate prediction of flows in a river such as caused by flood events, dam break, etc. is important because of the huge impacts on property, human life and environment. Several numerical difficulties must be adequately treated to obtain an accurate solution without numerical errors. Zhao *et al.* [5] provided a good historic revision and the features required for a 2D river flow simulation model: it must be able to handle complex topography, dry bed advancing fronts, wetting–drying moving boundaries, high roughness values, steady or unsteady flow and subcritical or supercritical conditions.

Natural topographies involve positive and negative bed slopes that can be steep in many places (mountainous areas) and abrupt banks. The presence of extreme slopes, high roughness and strong changes in the irregular geometry represent a great difficulty that can lead to important numerical errors presumably arising from the source terms discretization [6, 7] and the treatment of the wetting–drying fronts.

Flow over dry bed involves a complicated boundary condition which is dynamically changing in time with the moving front and continuously expanding or reducing the flow domain. Akanbi and Katopodes [8] gave a brief summary of problems encountered in the numerical simulation of flood waves propagating over dry bed. This is related to a theoretical and numerical difficulty because the shallow water system of equations loses its properties at $h = 0$ [8].

On the other hand, there has been little amount of research devoted to numerical treatment of the wetting and drying boundary. Flooding and drying arises in a wide range of free surface hydraulic problems, such as tidal floods, dam breaks and overland flow of precipitation. Cells being flooded or dried during the computation tend to introduce numerical instabilities in the solution, resulting for example in negative water depths or unphysical high velocities. Hence, different techniques have been proposed to handle it. These techniques include deformable computational meshes, modified equations in very shallow regions [9], and shock capturing schemes [10] considering that a cell is dry if water depth is below a small critical value (2 cm) [11]. Beffa and Connel [12] reported numerical oscillations when cells switch from dry to wet or *vice versa*. George and Stripling [13] represented the local bathymetry in each cell by a sloping facet rather than by a flat bed to eliminate the spurious shocks in their finite volume model. Some authors working with finite elements solve the problem allowing the controlled use of negative depths [14–16]. Bradford and Sanders [17] use Neumann extrapolation of the velocity in partially wet cells to bypass the incorrectly estimation of pressure and body forces in such cells.

Apart from the numerical stability, global mass or volume conservation is greatly affected by the careless treatment of the wetting/drying boundaries. There is a need for more work on model development for large scale complex natural river and flood plain flow simulation.

In a previous work, a 2D model was presented for unsteady flow simulation based on an explicit upwind finite volume method. Working on unstructured meshes, it was suitable for discontinuous and mixed flow regimes. The wetting/drying problem was included from a still water steady-state approach [18] and the requirement of exact mass conservation at the discrete level. Numerical error was still detected in presence of general situations. The objective of this work is to investigate in more detail the requirements linked to discrete mass conservation at wet/dry interfaces for all kind of situations. The analysis will be presented in the context of the upwind method used and applied to show the performance of the new approach.

2. MATHEMATICAL MODEL: 2D SHALLOW WATER SYSTEM OF EQUATIONS

Fluid flow is governed by mass conservation, Newton's second law and energy conservation. All these principles can be expressed in mathematical equations, in the form of partial derivatives. A very common hypothesis is the hydrostatic approximation valid for long waves (small vertical accelerations). When the horizontal direction is much greater than the vertical one, the mathematical model can be simplified averaging the 3D Navier–Stokes system of equations in depth and the problem is converted into a bidimensional one (2D shallow water model). This model describes appropriately some free surface problems. The shallow water system of equations is similar to the Euler system of equations that governs inviscid compressible flow in gas dynamics. Compressibility is equivalent to free surface deformability and Mach number is equivalent to Froude number. This property justifies the use of the same numerical techniques to solve the two systems of equations.

Neglecting diffusion of momentum due to viscosity and turbulence, wind effects and the Coriolis term, the 2D shallow water form the following system of equations:

$$\frac{\partial \mathbf{U}}{\partial t} + \frac{\partial \mathbf{F}(\mathbf{U})}{\partial x} + \frac{\partial \mathbf{G}(\mathbf{U})}{\partial y} = \mathbf{S}(x, y, \mathbf{U}) \tag{1}$$

in which,

$$\mathbf{U} = (h, q_x, q_y)^{\mathrm{T}}$$

$$\mathbf{F} = \left(q_x, \frac{q_x^2}{h} + \frac{gh^2}{2}, \frac{q_x q_y}{h}\right)^{\mathrm{T}}$$

$$\mathbf{G} = \left(q_y, \frac{q_x q_y}{h}, \frac{q_y^2}{h} + \frac{gh^2}{2}\right)^{\mathrm{T}}$$

where $q_x = uh$ and $q_y = vh$ are the unitary water discharges in x and y directions, respectively. The variable h represents the water depth, g is the acceleration of gravity and (u, v) are the depth averaged components of the velocity $\mathbf{u} = (u, v)$ along the x and y co-ordinates, respectively. $\mathbf{U}$ represents the vector of conserved variables and $\mathbf{F}$, $\mathbf{G}$ the fluxes associated to the conserved variables in both directions x and y. The source terms in the momentum equation ($\mathbf{S}$) are the bed slopes and the friction loses along the two co-ordinate directions,

$$\mathbf{S} = (0, gh(S_{0x} - S_{fx}), gh(S_{0y} - S_{fy}))^{\mathrm{T}}$$

where

$$S_{0x} = -\frac{\partial z}{\partial x}, \quad S_{0y} = -\frac{\partial z}{\partial y}$$

and the friction loses in terms of the Manning's roughness coefficient (n) [19]

$$S_{fx} = \frac{n^2 u\sqrt{u^2 + v^2}}{h^{4/3}}, \quad S_{fy} = \frac{n^2 v\sqrt{u^2 + v^2}}{h^{4/3}}$$

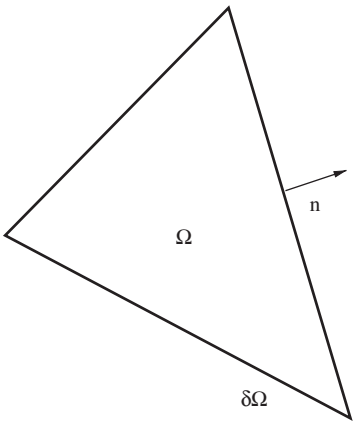

Figure 1. Details of a computational cell (finite volume Ω and surface surrounding the volume $\partial\Omega$).

It is useful to rewrite (1) as

$$\frac{\partial \mathbf{U}}{\partial t} + \boldsymbol{\nabla} \cdot \mathbf{E}(\mathbf{U}) = \mathbf{S}(x, y, \mathbf{U}) \tag{2}$$

in which $\mathbf{E} = (\mathbf{F}, \mathbf{G})^{\mathrm{T}}$ is the flux tensor, in order to introduce the integral form of the equations over a fixed volume Ω,

$$\frac{\partial}{\partial t} \int_{\Omega} \mathbf{U} \, \mathrm{d}\Omega + \int_{\Omega} (\boldsymbol{\nabla} \cdot \mathbf{E}) \, \mathrm{d}\Omega = \int_{\Omega} \mathbf{S} \, \mathrm{d}\Omega \tag{3}$$

In the 2D approach presented in this work, the spatial domain of integration is covered by a set of quadrilateral or triangular cells, not necessarily aligned with the co-ordinate directions. A discrete approximation to (3) is applied in every cell Ω_i so that the volume integrals represent integrals over the area of the cell with the dependent variables represented as piecewise constants and the surface integrals represent the total flux through the cell boundaries. Denoting by $\mathbf{U}_i$ the average value of the conservative variables over the volume Ω_i at a given time, from (3) and applying Gauss theorem to the second integral the following conservation equation can be written for every cell (Figure 1):

$$\frac{\partial \mathbf{U}_i}{\partial t} A_i + \oint_{\partial \Omega_i} (\mathbf{E} \cdot \mathbf{n}) \, \mathrm{d}s = \int_{\Omega_i} \mathbf{S} \, \mathrm{d}\Omega \tag{4}$$

where A_i is the area of the cell Ω_i.

The Jacobian matrix, $\mathbf{J}_{\mathbf{n}}$, of the normal flux $(\mathbf{E} \cdot \mathbf{n})$ is evaluated as

$$\mathbf{J}_{\mathbf{n}} = \frac{\partial (\mathbf{E} \cdot \mathbf{n})}{\partial \mathbf{U}} = \frac{\partial \mathbf{F}}{\partial \mathbf{U}} n_x + \frac{\partial \mathbf{G}}{\partial \mathbf{U}} n_y \tag{5}$$

and can be expressed as

$$\mathbf{J_n} = \begin{pmatrix} 0 & n_x & n_y \\ \left(gh - \frac{q_x^2}{h^2}\right) n_x - \frac{q_x q_y}{h^2} n_y & \frac{q_y}{h} n_y + \frac{2q_x}{h} n_x & \frac{q_x}{h} n_y \\ \left(gh - \frac{q_y^2}{h^2}\right) n_y - \frac{q_x q_y}{h^2} n_x & \frac{q_y}{h} n_x & \frac{q_x}{h} n_x + \frac{2q_y}{h} n_y \end{pmatrix}$$

The eigenvalues of $\mathbf{J_n}$ are a representation of the characteristic speeds

$$\begin{aligned} \lambda^1 &= un_x + vn_y + c \\ \lambda^2 &= un_x + vn_y \\ \lambda^3 &= un_x + vn_y - c \end{aligned} \tag{6}$$

where $c = \sqrt{gh}$ is the celerity of the small amplitude surface waves.

The corresponding eigenvectors are

$$\mathbf{e}^1 = \begin{pmatrix} 1 \\ u + cn_x \\ v + cn_y \end{pmatrix}, \quad \mathbf{e}^2 = \begin{pmatrix} 0 \\ -cn_y \\ cn_x \end{pmatrix}, \quad \mathbf{e}^3 = \begin{pmatrix} 1 \\ u - cn_x \\ v - cn_y \end{pmatrix} \tag{7}$$

From its eigenvectors, two matrices $\mathbf{P}$ and $\mathbf{P}^{-1}$ can be constructed with the property that they diagonalize the Jacobian $\mathbf{J_n}$

$$\mathbf{J_n} = \mathbf{P}\boldsymbol{\Lambda}\mathbf{P}^{-1}$$

where $\boldsymbol{\Lambda}$ is a diagonal matrix with eigenvalues in the main diagonal.

$$\boldsymbol{\Lambda} = \begin{pmatrix} un_x + vn_y + c & 0 & 0 \\ 0 & un_x + vn_y & 0 \\ 0 & 0 & un_x + vn_y - c \end{pmatrix}$$

The matrices which diagonalize the Jacobian have the form

$$\mathbf{P} = \begin{pmatrix} 1 & 0 & 1 \\ u + cn_x & -cn_y & u - cn_x \\ v + cn_y & cn_x & v - cn_y \end{pmatrix}, \quad \mathbf{P}^{-1} = \frac{1}{2c} \begin{pmatrix} \mathbf{u}\cdot\mathbf{n} + c & n_x & n_y \\ 2(un_y - vn_x) & -2n_y & 2n_x \\ \mathbf{u}\cdot\mathbf{n} + c & -n_x & v - n_y \end{pmatrix}$$

and

$$\Delta(\mathbf{E}\cdot\mathbf{n}) = \mathbf{J_n}\Delta\mathbf{U} = \mathbf{P}\boldsymbol{\Lambda}\mathbf{P}^{-1}\Delta\mathbf{U} = \mathbf{P}(\boldsymbol{\Lambda}^+ + \boldsymbol{\Lambda}^-)\mathbf{P}^{-1}\Delta\mathbf{U} \tag{8}$$

is the basis of the upwind method with $\boldsymbol{\Lambda}^{\pm} = (\boldsymbol{\Lambda} \pm |\boldsymbol{\Lambda}|)/2$.

3. EXPLICIT FIRST-ORDER UPWIND NUMERICAL SCHEME

The main reason to choose a first-order upwind flux and bed slope source term discretization for the shallow water equations on unstructured meshes is due to the simplicity of the numerical model, accuracy on the results and CPU time economy.

Upwind schemes are based on the idea of discretizing the spatial derivatives so that information is taken from the side it comes. Hence, a sense of propagation is implied and these techniques are well adapted to advection dominated problems. When source terms are present, it has previously been shown [6, 20–23] that the flux derivatives and the source terms have to be discretized in a similar manner. The evaluation of fluxes and sources at the same local state is important. The basic technique will be outlined next for completeness.

The local definition of an approximated flux Jacobian, $\tilde{\mathbf{J}}_{\mathrm{RL}}$, constructed at the edges of the cells is exploited here. Formally it is analogous to $\mathbf{J}_{\mathbf{n}}$ (5) but it is expressed in terms of averaged quantities across a cell edge RL, associated to the normal direction $\mathbf{n}$.

As suggested by Roe [24] the matrix $\tilde{\mathbf{J}}_{\mathrm{RL}}$ has the same shape as $\mathbf{J}_{\mathbf{n}}$ but is evaluated at an average state given by the quantities $\tilde{\mathbf{u}} = (\tilde{u}, \tilde{v})$ and $\tilde{c}$ which must be calculated according to the matrix properties [25].

The possibility of splitting the diagonal form of the Jacobian and the approximated Jacobian into positive (outward) and negative (inward) components has been used and is the basis of upwind schemes. When solving cell by cell, only the incoming contributions are taken into account and this is linked to the $\tilde{\mathbf{\Lambda}}^{-}$ component due to the sign convention for the normal to the cell. Hence, (4) can be discretized as follows:

$$\mathbf{U}_i^{n+1} = \mathbf{U}_i^n - \frac{\Delta t}{A_i}\left(\sum_{k=1}^{NE} (\tilde{\mathbf{P}}\tilde{\mathbf{\Lambda}}^{-}\tilde{\mathbf{P}}^{-1}\Delta\mathbf{U})_k \, ds_k\right)_i^n + \frac{\Delta t}{A_i}\int_{\Omega_i} \mathbf{S}\,\mathrm{d}\Omega \tag{9}$$

where k represents the edge index of the cell Ω_i, NE is the total number of edges in the cell ($NE = 3$ for triangles, $NE = 4$ for quadrilaterals). The vector $\mathbf{n}_k$ is the unit outward normal and ds_k is the length of the side.

Alternatively, it is very common in finite volume techniques the definition and use of a numerical flux associated to every scheme. This is a convenient auxiliary quantity coming from the control volume theory.

The evaluation of the numerical flux used in this work derives from (9),

$$\mathbf{E}_k^* \cdot \mathbf{n}_k = (\mathbf{F}, \mathbf{G})_k^* \cdot \mathbf{n}_k = \tfrac{1}{2}[(\mathbf{F}, \mathbf{G})_{\mathrm{R}} \cdot \mathbf{n} + (\mathbf{F}, \mathbf{G})_{\mathrm{L}} \cdot \mathbf{n} - |\tilde{\mathbf{J}}_{\mathrm{RL}}|(\mathbf{U}_{\mathrm{R}} - \mathbf{U}_{\mathrm{L}})] \tag{10}$$

Note that subscript k will be omitted for the sake of clarity and the following discussion is referred to the cell side k.

The approximate Jacobian matrix is not directly used in the actual method. Instead, the difference in the vector $\mathbf{U}$ across the grid edge is decomposed on the matrix eigenvectors basis as

$$\Delta\mathbf{U} = \mathbf{U}_{\mathrm{R}} - \mathbf{U}_{\mathrm{L}} = \sum_{m=1}^{3} \alpha^m \tilde{\mathbf{e}}^m \tag{11}$$

and

$$|\tilde{\mathbf{J}}_{\mathrm{RL}}|(\mathbf{U}_{\mathrm{R}} - \mathbf{U}_{\mathrm{L}}) = \sum_{m=1}^{3} |\tilde{\lambda}^m| \alpha^m \tilde{\mathbf{e}}^m \tag{12}$$

where the expression of coefficients α^m are [25]

$$\begin{aligned}\alpha^{1,3} &= \frac{h_R - h_L}{2} \pm \frac{1}{2\tilde{c}}[((hu)_R - (hu)_L)n_x \\ &\quad + ((hv)_R - (hv)_L)n_y - (\tilde{u}n_x + \tilde{v}n_y)(h_R - h_L)] \\ \alpha^2 &= \frac{1}{\tilde{c}}[((hv)_R - (hv)_L - \tilde{v}(h_R - h_L))n_x \\ &\quad - ((hv)_R - (hv)_L - \tilde{u}(h_R - h_L))n_y]\end{aligned} \tag{13}$$

From the eigenvalues of $\mathbf{J}$, those of $\tilde{\mathbf{J}}_{RL}$ have form (6) satisfying the following entropy condition:

$$\text{if} \quad |\tilde{\lambda}^{1,3}| < \varepsilon^{1,3} \rightarrow |\tilde{\lambda}^{1,3}| = \varepsilon^{1,3} \tag{14}$$

being

$$\varepsilon^{1,3} = \max(0, \tilde{\lambda}^{1,3} - \lambda_L^{1,3},\ \lambda_R^{1,3} - \tilde{\lambda}^{1,3}) \tag{15}$$

and the eigenvectors have the form (7), all in terms of average velocities and celerity. Enforcing the second condition [25] of the matrix $\tilde{\mathbf{J}}_{RL}$ the following expressions for $\tilde{u}$, $\tilde{v}$ and $\tilde{c}$ can be obtained:

$$\tilde{u} = \frac{\sqrt{h_R}u_R + \sqrt{h_L}u_L}{\sqrt{h_R} + \sqrt{h_L}}, \quad \tilde{v} = \frac{\sqrt{h_R}v_R + \sqrt{h_L}v_L}{\sqrt{h_R} + \sqrt{h_L}}, \quad \tilde{c} = \sqrt{\frac{g}{2}(h_R + h_L)} \tag{16}$$

Expression (10) provides the numerical flux normal to each edge of the computational cells so that (4) becomes

$$\mathbf{U}_i^{n+1} = \mathbf{U}_i^n - \frac{\Delta t}{A_i}\left(\sum_{k=1}^{NE} \mathbf{E}_k^* \cdot \mathbf{n}_k\, ds_k\right)_i^n + \frac{\Delta t}{A_i}\int_{\Omega_i} \mathbf{S}\, d\Omega \tag{17}$$

A cellwise numerical source, $\mathbf{S}^*$, can be defined as an approach of the integral of the source term $\int_{\Omega_i} \mathbf{S}\, d\Omega$.

An upwind approach adopted to model the bottom variations was presented by Brufau *et al.* [18] and reproduced here for the sake of completeness. It ensures the best balance with the flux terms at least in steady cases. This procedure was studied in detail by Bermúdez and Vázquez-Cendón [6].

On the other hand, for every cell-edge k of cell Ω_i the discrete source term, $\tilde{\mathbf{S}}_k$, is decomposed into inward and outward contributions

$$\tilde{\mathbf{S}}_k = \tilde{\mathbf{S}}_k^+ + \tilde{\mathbf{S}}_k^-$$

being

$$\tilde{\mathbf{S}}_k^\pm = \tfrac{1}{2}\,\tilde{\mathbf{P}}(\mathbf{I} \pm |\tilde{\mathbf{\Lambda}}|\tilde{\mathbf{\Lambda}}^{-1})\tilde{\mathbf{P}}^{-1}\tilde{\mathbf{S}}_k = \sum_{m=1}^{3} \beta^{m\pm}\tilde{\mathbf{e}}^m \tag{18}$$

For every cell Ω_i the total contribution of the edge source terms to the cell source term, $\mathbf{S}^*$, is made of the sum of the parts associated to inward normal velocity at every edge k

$$\mathbf{S}^* = \int_{\Omega_i} \mathbf{S}\,\mathrm{d}\Omega = \sum_{k=1}^{NE} \tilde{\mathbf{S}}_k^- \, ds_k$$

The expressions for the β^- coefficients are

$$\begin{aligned} \beta^{1-,3-} &= \pm\frac{1}{4\tilde{c}}(1-\mathrm{sign}(\tilde{\lambda}^{1,3}))[\bar{\mathbf{S}}_2 n_x + \bar{\mathbf{S}}_3 n_y] d_{\mathrm{RL}} \\ \beta^{2-} &= \frac{1}{2\tilde{c}}(1-\mathrm{sign}(\tilde{\lambda}^{2}))[-\bar{\mathbf{S}}_2 n_y + \bar{\mathbf{S}}_3 n_x] d_{\mathrm{RL}} \end{aligned} \tag{19}$$

where $\bar{\mathbf{S}}_{2,3}$ are the second and third components of the vector of source terms $\bar{\mathbf{S}}$. Applying it to the bed slope source term,

$$\bar{\mathbf{S}} = \begin{pmatrix} 0 \\ g\tilde{h}\Delta z_x \\ g\tilde{h}\Delta z_y \end{pmatrix}_k \tag{20}$$

where $\tilde{h}$ consists of the average obtained from the depth values stored in the left and right cell that share the same edge in each computational cell:

$$\tilde{h} = \tfrac{1}{2}(h_{\mathrm{R}} + h_{\mathrm{L}}) \tag{21}$$

and the bed increments in each direction are computed in the form

$$\Delta z_x = -\frac{(z_{\mathrm{R}} - z_{\mathrm{L}})}{d_{\mathrm{RL}}} n_x, \quad \Delta z_y = -\frac{(z_{\mathrm{R}} - z_{\mathrm{L}})}{d_{\mathrm{RL}}} n_y \tag{22}$$

where d_{RL} is the distance between the centroids of the right (R) and left (L) cells that share the same edge.

The average value, (20), proposed in Bermúdez *et al.* [21], ensures a conservative discretization of this source term.

In general, the friction term can be discretized in a semi-implicit manner to avoid numerical oscillations when the roughness coefficient is high; so that, the final expression for the numerical scheme is

$$\mathbf{U}_i^{n+1} = \frac{\mathbf{U}_i^n - (\Delta t/A_i)\left(\sum_{k=1}^{NE}(\mathbf{E}_k^* \cdot \mathbf{n}_k - \tilde{\mathbf{S}}_k^{1-})ds_k\right)_i^n + (\Delta t/A_i)\theta(\mathbf{S}^2)_i^n}{1-(1-\theta)(\Delta t/A_i)(\mathbf{S}^2)_i^n/\mathbf{U}_i^n} \tag{23}$$

in which θ is the implicitness degree of the friction term discretization: $\theta = 1$ corresponds to a totally explicit treatment and $\theta = 0$ to a totally implicit one. Although in Equation (23)

velocity appears dividing the source term, it is there only for formal reasons. In practical use the velocity is cancelled with the velocity of friction loses (Equation (2)) and division by zero velocity is avoided.

The stability criterion adopted has followed the usual in explicit finite volumes [25] for the homogeneous system of equations not including source terms

$$\Delta t = \mathrm{CFL}\,\frac{A_i}{(\sqrt{u^2+v^2}+\sqrt{gh})P_i} \tag{24}$$

where P_i and A_i are the perimeter and area, respectively, of the computational cell i. In practice, some restrictions on the CFL can be observed due to the non-linearity of the system of equations or to the presence of source terms. Theoretical studies on this question are still on development.

4. WETTING–DRYING CONDITION FOR STEADY AND UNSTEADY FLOW

The numerical technique described in Section 3 is an approximate Riemann solver adapted to cope with zero depth cells which provides a discrete solution to the problem in all cases independently of the local bed slope value. The technique is unable to solve correctly some situations of still water in presence of adverse slopes as pointed out by Brufau *et al.* [18]. On the other hand, the basic method can lead to important errors when simulating flow movement over high slopes of both positive and negative signs. In what follows, this statement will be developed and a quantification of the problematic slopes will be presented.

In finite volume-based shallow water models, moving boundaries are considered as wetting/drying fronts and hence included in the ordinary cell procedure in a through calculation that assumes zero water depth for the dry cells. A cell is considered dry if the water depth in the cell is below 10^{-6} m. A numerical technique based on the discrete form of the mass conservation equation which guarantees steady-state at the wet/dry front was proposed by Brufau *et al.* [18] to avoid difficulties in advances over adverse slopes for steady problems. Now, in this work, a new WDC is proposed intended to be valid for steady or unsteady cases and leading to zero numerical errors in the transient computations. The new WDC includes the WDC for steady flow presented by Brufau *et al.* [18] as a particular case.

In the upper part of Figure 2 water and bottom surface in a real situation are plotted and at the lower part their discrete representation with constant functions z and H over the cells.

A more general alternative is adapted here, in order to avoid the numerical error, forcing the mass balance by means of a modification of the bed slope consisting on the local redefinition of the bottom level difference at the interface to fulfil the mass conservation equation. For the sake of simplicity in the discussion, let us consider the cell interface LR where the R cell is assumed dry and the L cell is wet with non-zero velocity in general (Figure 2 top).

$$\begin{aligned} h_{\mathrm{L}} &\neq 0, \quad h_{\mathrm{R}} = 0 \\ u_{\mathrm{L}} &\neq 0, \quad u_{\mathrm{R}} = 0 \\ v_{\mathrm{L}} &\neq 0, \quad v_{\mathrm{R}} = 0 \end{aligned} \tag{25}$$

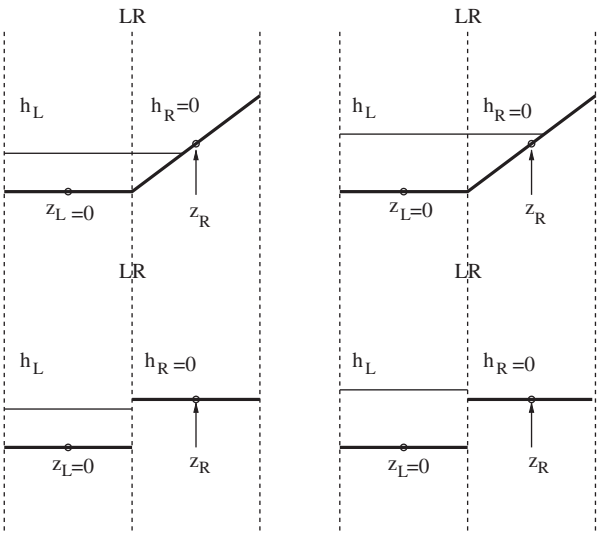

Figure 2. Wetting/drying fronts over adverse steep slopes in real (up) and discrete (down) representations which require a modification (left) or not (right).

Following the upwind numerical scheme presented in Section 3, the averaged celerity and velocities at LR interface are

$$\begin{aligned} \tilde{u} &= u_{\mathrm{L}} \\ \tilde{v} &= v_{\mathrm{L}} \\ \tilde{c} &= \sqrt{(g/2)h_{\mathrm{L}}}, \end{aligned} \tag{26}$$

the coefficients α have the form

$$\begin{aligned} \alpha^{1,3} &= -\frac{h_{\mathrm{L}}}{2} \\ \alpha^{2} &= \frac{1}{\tilde{c}}[h_{\mathrm{L}}v_{\mathrm{L}}n_x - h_{\mathrm{L}}u_{\mathrm{L}}n_y] \end{aligned} \tag{27}$$

The eigenvalues are

$$\begin{aligned} \tilde{\lambda}^1 &= \tilde{\mathbf{u}}\cdot\mathbf{n} + \tilde{c} = \tilde{u}n_x + \tilde{v}n_y + \tilde{c} = u_{\mathrm{L}}n_x + v_{\mathrm{L}}n_y + \sqrt{\frac{g}{2}h_{\mathrm{L}}} \\ \tilde{\lambda}^2 &= \tilde{\mathbf{u}}\cdot\mathbf{n} = \tilde{u}n_x + \tilde{v}n_y = u_{\mathrm{L}}n_x + v_{\mathrm{L}}n_y \\ \tilde{\lambda}^3 &= \tilde{\mathbf{u}}\cdot\mathbf{n} - \tilde{c} = \tilde{u}n_x + \tilde{v}n_y - \tilde{c} = u_{\mathrm{L}}n_x + v_{\mathrm{L}}n_y - \sqrt{\frac{g}{2}h_{\mathrm{L}}} \end{aligned} \tag{28}$$

Using (23) with $\theta = 0$, and considering only the first component, i.e. the discretization of the mass conservation equation, the following expression follows:

$$\frac{h_{\mathrm{L}}^{n+1} - h_{\mathrm{L}}^{n}}{\Delta t} = -\frac{1}{A}\sum_{k=1}^{NE}(\mathbf{E}_k^{*}\cdot\mathbf{n}_k - \tilde{\mathbf{S}}_k^{-})^1 ds_k \tag{29}$$

4.1. Subcritical flow

In case of subcritical flow, $\tilde{\mathbf{u}}\mathbf{n} < \tilde{c}$ so

$$\begin{aligned} \tilde{\lambda}^1 > 0 \;\Rightarrow\; |\tilde{\lambda}^1| &= \tilde{\lambda}^1 \\ \tilde{\lambda}^3 < 0 \;\Rightarrow\; |\tilde{\lambda}^3| &= -\tilde{\lambda}^3 \end{aligned} \tag{30}$$

The numerical flux at the LR edge is evaluated as

$$\begin{aligned} \mathbf{E}^* \cdot \mathbf{n} = \tfrac{1}{2}[&\mathbf{F}_\mathrm{R} n_x + \mathbf{G}_\mathrm{R} n_y + \mathbf{F}_\mathrm{L} n_x + \mathbf{G}_\mathrm{L} n_y - |\tilde{\lambda}^1|\alpha^1 \tilde{\mathbf{e}}^1 \\ &- |\tilde{\lambda}^2|\alpha^2 \tilde{\mathbf{e}}^2 - |\tilde{\lambda}^3|\alpha^3 \tilde{\mathbf{e}}^3] \end{aligned} \tag{31}$$

For the first component of the system of equations, i.e. mass equation, substituting eigenvalues, eigenvectors, coefficients and fluxes in (31) we obtain

$$\begin{aligned} (\mathbf{E}^* \cdot \mathbf{n})^1 &= \tfrac{1}{2}[(hu)_\mathrm{L} n_x + (hv)_\mathrm{L} n_y - |\tilde{\lambda}^1|\alpha^1 \cdot 1 - |\tilde{\lambda}^2|\alpha^2 \cdot 0 - |\tilde{\lambda}^3|\alpha^3 \cdot 1] \\ &= \frac{1}{2}\left[(hu)_\mathrm{L} n_x + (hv)_\mathrm{L} n_y + (\tilde{\mathbf{u}}\mathbf{n} + \tilde{c})\frac{h_\mathrm{L}}{2} + (-\tilde{\mathbf{u}}\mathbf{n} + \tilde{c})\frac{h_\mathrm{L}}{2}\right] \\ &= \frac{h_\mathrm{L}}{2}[u_\mathrm{L} n_x + v_\mathrm{L} n_y + \tilde{c}] = \frac{h_\mathrm{L}}{2}[\tilde{\mathbf{u}}\mathbf{n} + \tilde{c}] \end{aligned} \tag{32}$$

The source term contribution of the bed slope to the mass equation is governed by

$$\begin{aligned} &\beta^{1-} \cdot 1 + \beta^{2-} \cdot 0 + \beta^{3-} \cdot 1 \\ &= -\frac{1}{2\tilde{c}}\left[\bar{\mathbf{S}}_2 n_x + \bar{\mathbf{S}}_3 n_y\right] d_\mathrm{RL} \\ &= -\frac{1}{2\tilde{c}}[g\tilde{h}\Delta z_x n_x + g\tilde{h}\Delta z_y n_y] d_\mathrm{RL} \\ &= \frac{1}{2\tilde{c}}\left[g\frac{h_\mathrm{L}}{2}(z_\mathrm{R} - z_\mathrm{L})\frac{n_x^2}{d_\mathrm{RL}} + g\frac{h_\mathrm{L}}{2}(z_\mathrm{R} - z_\mathrm{L})\frac{n_y^2}{d_\mathrm{RL}}\right] d_\mathrm{RL} \\ &= \frac{1}{2\tilde{c}} g\tilde{h}(z_\mathrm{R} - z_\mathrm{L}) = \frac{1}{2}\tilde{c}(z_\mathrm{R} - z_\mathrm{L}) \end{aligned} \tag{33}$$

Therefore, the total contribution from the fluxes and bed slope source term is

$$(\mathbf{E}^{*1}\cdot\mathbf{n}-\tilde{\mathbf{S}}^{1-})_{\mathrm{LR}}=\tfrac{1}{2}[h_{\mathrm{L}}(\tilde{\mathbf{u}}\mathbf{n}+\tilde{c})-\tilde{c}(z_{\mathrm{R}}-z_{\mathrm{L}})]$$

$$\begin{cases} =0 & \text{if} \quad (z_{\mathrm{R}}-z_{\mathrm{L}})=h_{\mathrm{L}}\left(1+\dfrac{\tilde{\mathbf{u}}\mathbf{n}}{\tilde{c}}\right) \\ >0 & \text{if} \quad (z_{\mathrm{R}}-z_{\mathrm{L}})<h_{\mathrm{L}}\left(1+\dfrac{\tilde{\mathbf{u}}\mathbf{n}}{\tilde{c}}\right) \\ <0 & \text{if} \quad (z_{\mathrm{R}}-z_{\mathrm{L}})>h_{\mathrm{L}}\left(1+\dfrac{\tilde{\mathbf{u}}\mathbf{n}}{\tilde{c}}\right) \end{cases} \tag{34}$$

Now, the three different cases obtained are going to be studied following the point of view of the wet cell (L). The contribution of the LR edge to updating the mass conservation equation is

$$A\left(\frac{h_{\mathrm{L}}^{n+1}-h_{\mathrm{L}}^{n}}{\Delta t}\right)_{\mathrm{LR}}=\frac{l}{2}[\tilde{c}(z_{\mathrm{R}}-z_{\mathrm{L}})-h_{\mathrm{L}}(\tilde{\mathbf{u}}\mathbf{n}+\tilde{c})] \tag{35}$$

being A the area and l the length of the wetting–drying edge of the wet cell. There are three cases depending on the bed level variation.

(1)

$$(z_{\mathrm{R}}-z_{\mathrm{L}})=(h_{\mathrm{L}})_{\mathrm{LR}}\left(1+\frac{\tilde{\mathbf{u}}\mathbf{n}}{\tilde{c}}\right) \;\Rightarrow\; (h_{\mathrm{L}}^{n+1})_{\mathrm{LR}}=(h_{\mathrm{L}}^{n})_{\mathrm{LR}} \tag{36}$$

There is no mass exchange between the wet and the dry cells. For still water steady flow, $u_{\mathrm{L}}=v_{\mathrm{L}}=0$, and the condition for the bed slope is reduced to $(z_{\mathrm{R}}-z_{\mathrm{L}})=h_{\mathrm{L}}$ which recovers the WDC developed for steady problems by Brufau *et al.* [18] following the work done by Bermúdez *et al.* [21] and taking into account that flux and source discretizations must balance to ensure still water steady-state at the interface LR.

(2)

$$(z_{\mathrm{R}}-z_{\mathrm{L}})<(h_{\mathrm{L}})_{\mathrm{LR}}\left(1+\frac{\tilde{\mathbf{u}}\mathbf{n}}{\tilde{c}}\right) \;\Rightarrow\; (h_{\mathrm{L}}^{n+1})_{\mathrm{LR}}<(h_{\mathrm{L}}^{n})_{\mathrm{LR}} \tag{37}$$

The wet cell loses water depth (mass) which goes to the dry cell. This case corresponds to downhill slopes ($z_{\mathrm{R}}-z_{\mathrm{L}}<0$) and moderate uphill slopes. In the first case, water flows from an upper to a lower cell moved both by inertia and gravity. It must be stressed here that there exists a threshold for the bed slope compatible with the numerical stability for a fixed time step. In other words, there is a limit for the bed slope for a given time step because at least all the water volume stored at the wet cell can be lost but no more. In adverse slope cases it does not represent a problem but otherwise the procedure can generate negative water depths in the wet cell. We shall come to this point later.

(3)

$$(z_{\mathrm{R}}-z_{\mathrm{L}})>(h_{\mathrm{L}})_{\mathrm{LR}}\left(1+\frac{\tilde{\mathbf{u}}\mathbf{n}}{\tilde{c}}\right) \;\Rightarrow\; (h_{\mathrm{L}}^{n+1})_{\mathrm{LR}}>(h_{\mathrm{L}}^{n})_{\mathrm{LR}} \tag{38}$$

Independently of the contributions from the other cell edges, this result implies that the wet cell is receiving water from the dry cell which is impossible because there is no water in the dry cell. This is the case in which the bed slope must be redefined locally for this time step to guarantee mass conservation in the form $(z_R - z_L) = (h_L)_{LR}(1 + \tilde{\mathbf{u}}\mathbf{n}/\tilde{c})$.

4.2. Supercritical flow

In case of supercritical flow, $\tilde{\mathbf{u}}\mathbf{n} > \tilde{c}$ so

$$\begin{aligned} \tilde{\lambda}^1 &> 0 \;\Rightarrow\; |\tilde{\lambda}^1| = \tilde{\lambda}^1 \\ \tilde{\lambda}^3 &> 0 \;\Rightarrow\; |\tilde{\lambda}^3| = \tilde{\lambda}^3 \end{aligned} \tag{39}$$

The numerical flux contribution to the mass equation in the wetting–drying edge using again (25)–(28) is

$$\begin{aligned} \mathbf{E}^{*1} \cdot \mathbf{n} &= \tfrac{1}{2}[(hu)_L n_x + (hv)_L n_y - |\tilde{\lambda}^1|\alpha^1 \cdot 1 - |\tilde{\lambda}^2|\alpha^2 \cdot 0 - |\tilde{\lambda}^3|\alpha^3 \cdot 1] \\ &= \frac{1}{2}\left[(hu)_L n_x + (hv)_L n_y + (\tilde{\mathbf{u}}\mathbf{n} + \tilde{c})\frac{h_L}{2} + (\tilde{\mathbf{u}}\mathbf{n} - \tilde{c})\frac{h_L}{2}\right] \\ &= h_L[u_L n_x + v_L n_y] = h_L \tilde{\mathbf{u}}\mathbf{n} \end{aligned} \tag{40}$$

The source term contribution of the bed slope to the mass equation is governed by

$$\beta^{1-} \cdot 1 + \beta^{2-} \cdot 0 + \beta^{3-} \cdot 1 = -\frac{1}{2\tilde{c}}[\bar{\mathbf{S}}_2 n_x + \bar{\mathbf{S}}_3 n_y] d_{RL} = 0 \tag{41}$$

There is no contribution of the bed slope source terms because the sign of the eigenvalues is positive in both cases, for β^{1-} and β^{3-}. In this case nothing has to be done as far as redefining the bed slope is concerned.

However, the supercritical case is not always free from errors. Depending on the cases, and always near fronts is presence of bed slopes, the discretization of the mass equation leads to negative depths arising from an excessive time step size as suggested above. The solution proposed here to get rid of these unphysical negative depths not changing the time step used and enforcing at the same time mass conservation is as follows: first, the cells with negative depth after one time step are identified and their water depth values and velocity components are put to zero which adds water to the global system. Then, in order to preserve mass conservation, the cells surrounding them are checked and the same volume of water is substracted from the neighbour having more water. Calling L a general cell with a negative water depth and R the neighbour cell with more water, the algorithm is as follows:

- h_R is redefined to $h_R + h_L A_L/A_R$ before h_L is set to zero taking into account the area since the unstructured cells are usually of different size.
- $h_L < 0$ is redefined as $h_L = 0$, involving an addition of a volume of water $A_L h_L$ to the system.

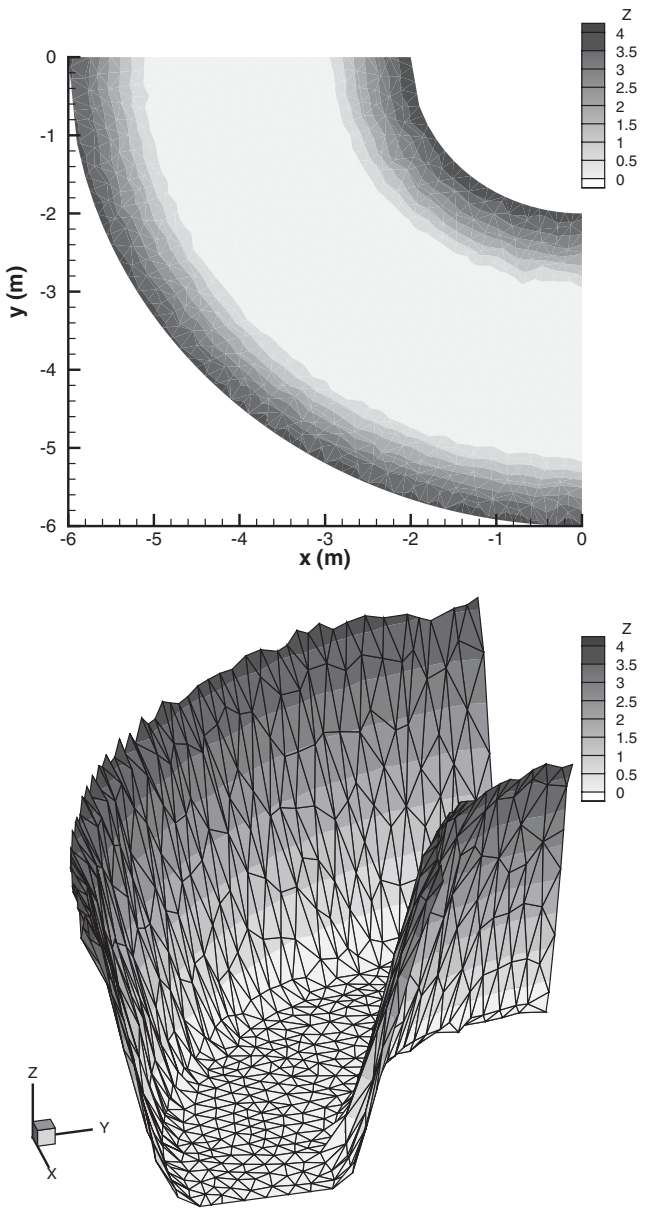

Figure 3. Plan view of the geometry of the curved channel (top). Contour plot of the bed levels (bottom).

With this new WDC and bed slope modification for unsteady flow together with the negative depths control in the calculation we have been able to eliminate all numerical errors of this kind in the discretization which was the objective to obtain an accurate numerical technique in mass conservation. Controlling negative depths we intend to help the numerical method in

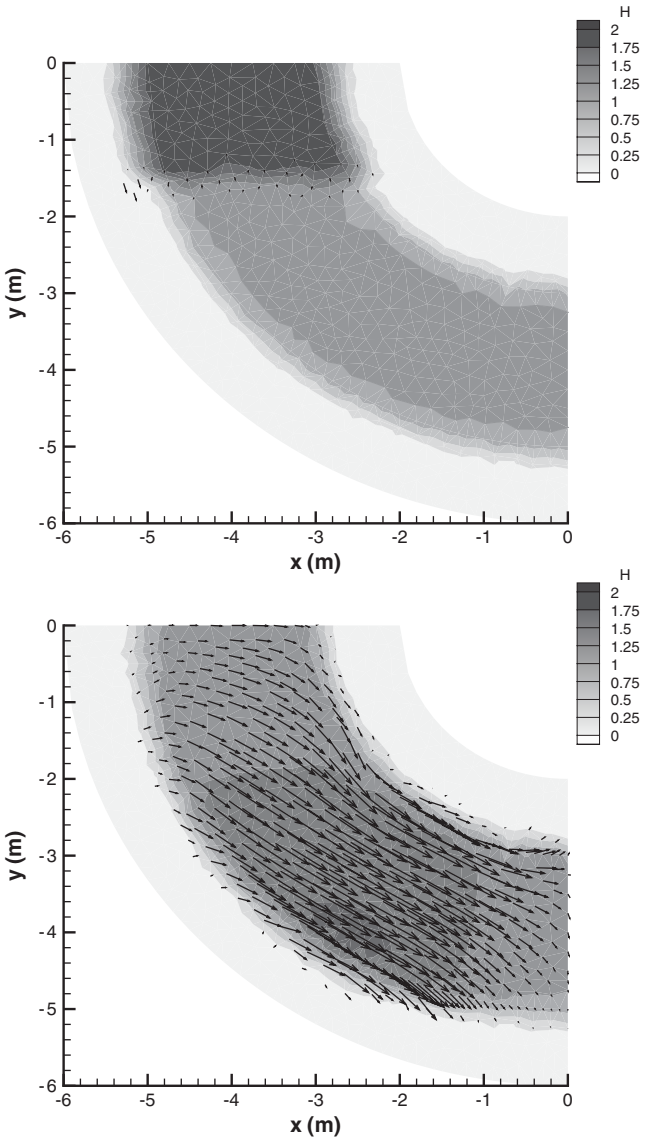

Figure 4. Contour plots of water depth and velocity vectors at time: $0, 1, 2, 4, 20$ and 120 s, CFL $= 0.9$. The last plot corresponds to steady state.

the process of drying. Sometimes the slope is very steep and the numerical method trying to dry the slope leads to negative depth in the drying cell. It is due to the fact that only one cell can be dried with this numerical method when in the same time step more than one cell should be dried. It is an economic way of helping the method to dry more than one cell without reducing the time step to very small values which would lead to large computational time.

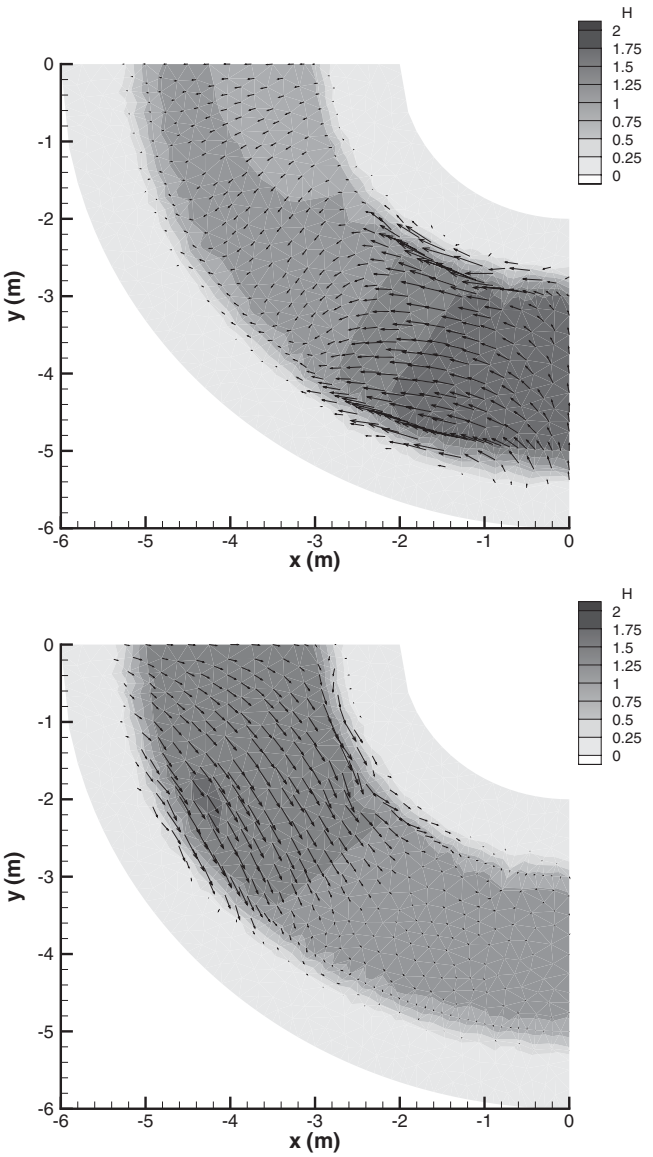

Figure 4. *Continued.*

5. PHYSICAL DOMAIN BOUNDARY CONDITIONS

The procedure described in the previous section is applied for the ordinary cells, that is, those representing points at the interior of the wetted domain. The boundaries of the wetted domain are defined by the cells not completely surrounded by other cells. All these cells actually require the definition of suitable boundary conditions in order to reach the solution

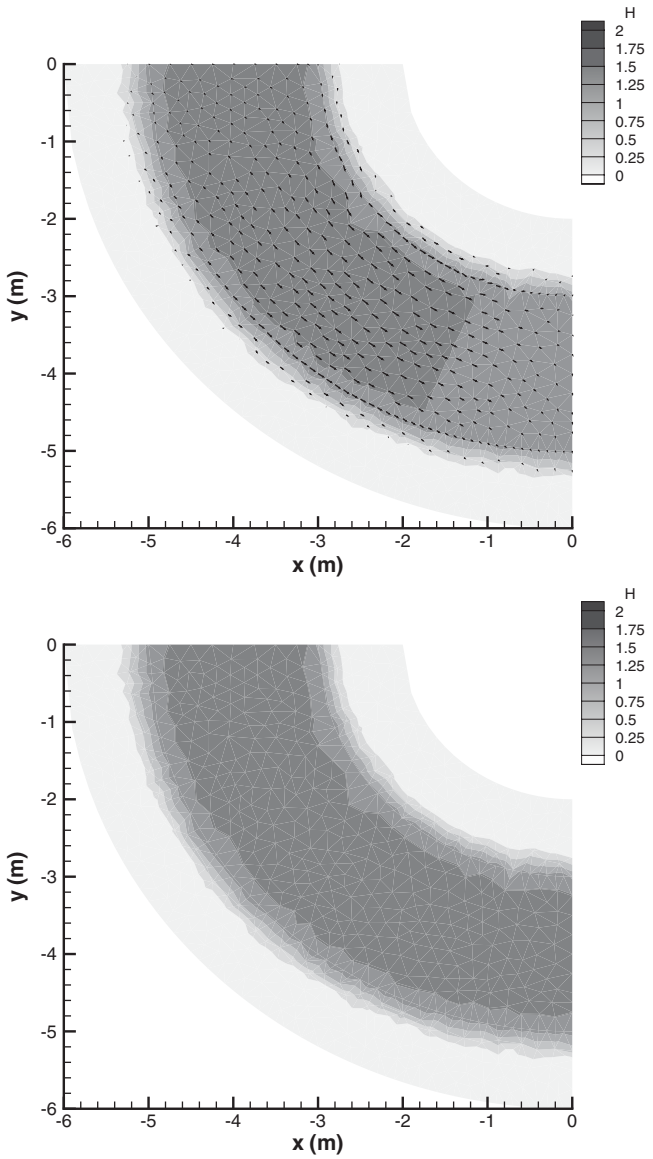

Figure 4. *Continued.*

of a problem. As in any other boundary problem in computational fluid dynamics, there is first a question concerning the number of physical boundary conditions required at every boundary point. To help, the theory of characteristics in 2D tells us that, depending on both the value of the normal velocity through the boundary

$$\mathbf{u} \cdot \mathbf{n} = un_x + vn_y \tag{42}$$

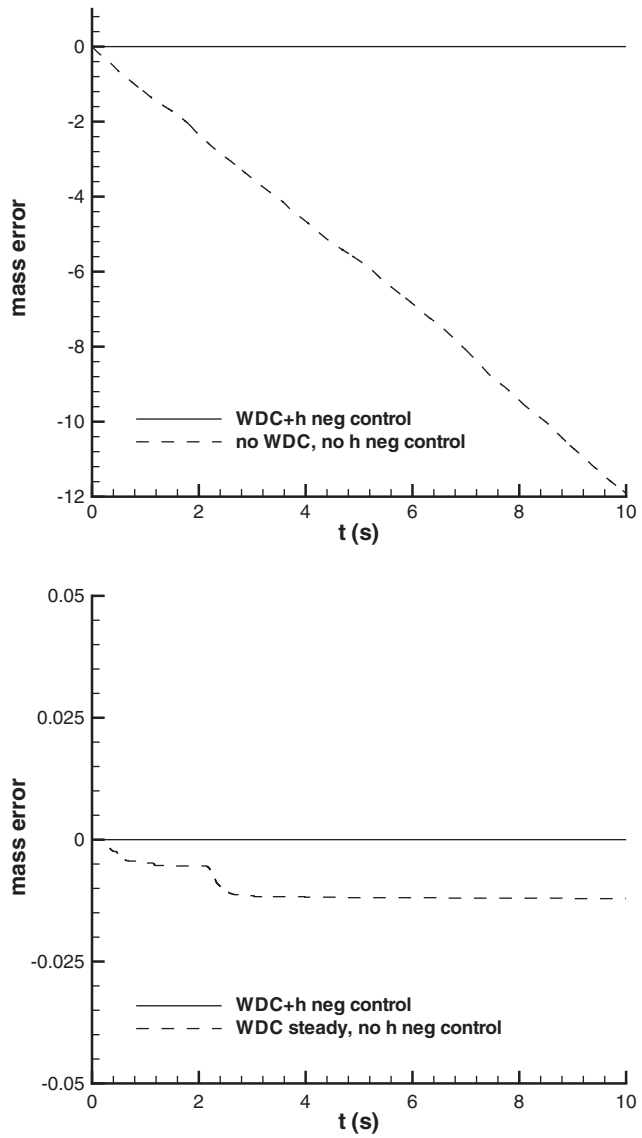

Figure 5. Time evolution of mass error (m^3) in the case of dam break over a curved trapezoidal channel using the unsteady WDC or the steady WDC or none.

and the local Froude number $Fr = (\mathbf{u} \cdot \mathbf{n})/c$, there are four possibilities as detailed in Hirsch [26].

A second question is related to the procedure used to obtain numerical boundary conditions [26]. In the work presented here, the idea of using a Riemann solver to calculate the flux at the edges of a cell has also been used at the boundaries. The variables are stored at the

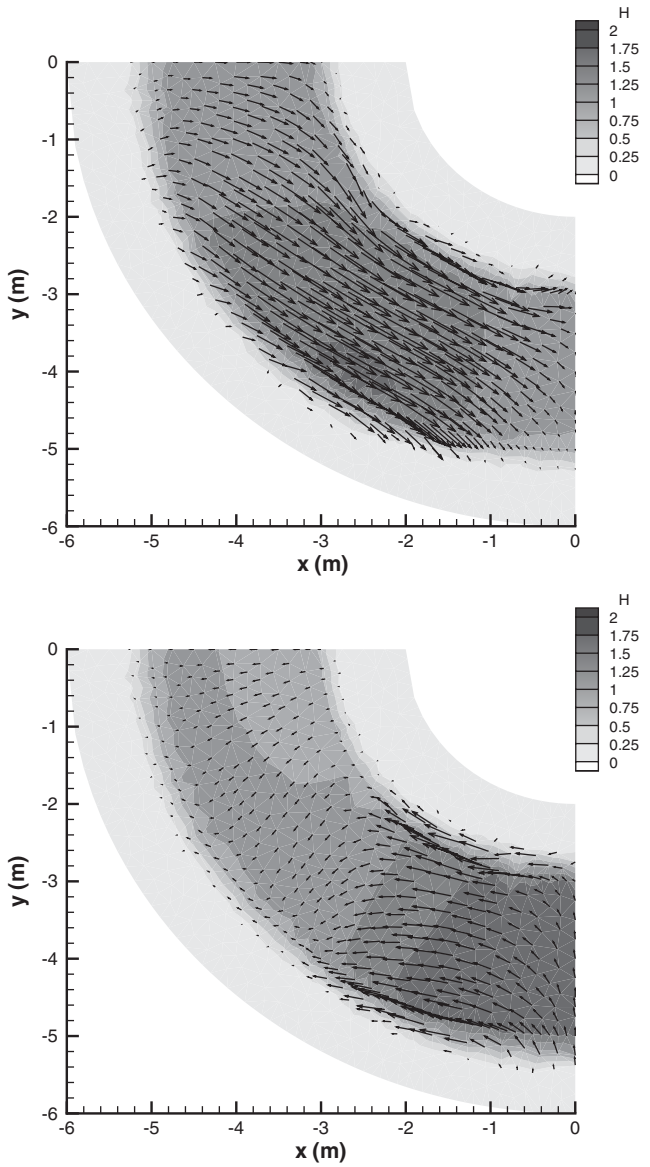

Figure 6. Contour plots of water depth and velocity vectors at time: $1, 2, 4$ and 20 s, CFL $= 0.1$.

centre of each cell and the boundary conditions are also imposed there, in boundary cells. The value of the variables not prescribed is calculated from a usual finite volume balance. For this purpose, the fluxes across the edges lying on the boundary are estimated by means of a 'ghost' outside cell. Usually, the ghost cell just duplicates the boundary cell (outflow cells). When the boundary is a solid wall, the ghost cell is a mirror cell in which the depth

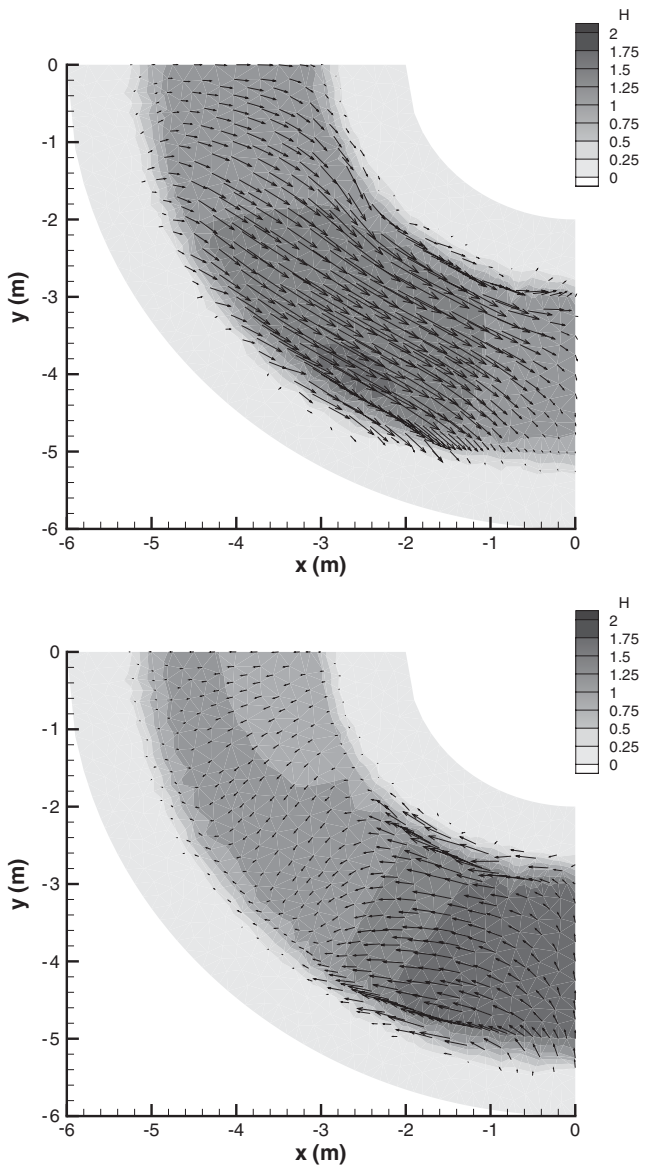

Figure 6. *Continued.*

of water has the same value as the boundary cell and the velocities have the opposite sign. The procedure is the same followed with the inside cells, Riemann problem is solved across the edges (without source terms) but after the computation, boundary conditions are imposed over the values calculated on the boundary cells. This step is needed because computing all the fluxes across all the edges that surround a boundary cell can make the imposed values change.

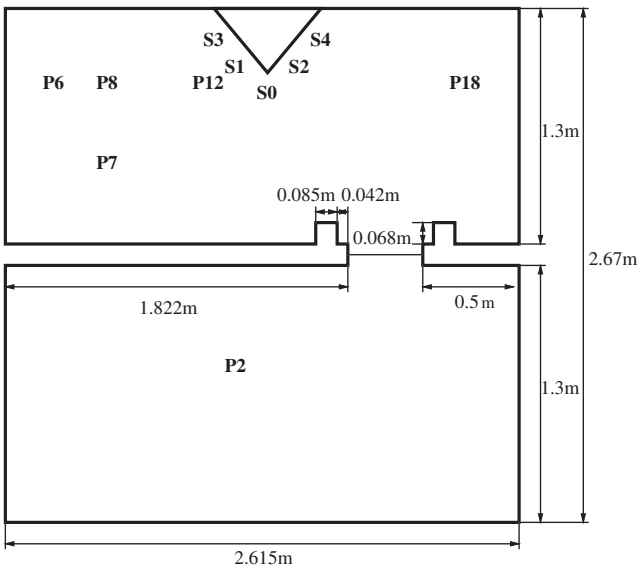

Figure 7. Plane view of the physical model which simulates a non-symmetric dam break in a pool with a pyramidal obstacle.

6. DAM BREAK ON A TRAPEZOIDAL CURVED CHANNEL

In order to focus on the performance of the WDC in subcritical cases, an academic example is proposed. It consists of a curved channel trapezoidal in cross section and closed at both upstream and downstream fixed boundaries. The unsteady flow is generated by a dam-break initial condition. In order to keep subcritical flow, the initial discontinuity in water depth is assumed small (2:1). The flow evolution involves wetting and drying of the channel banks as water moves in several reflections from the closed ends. Finally it tends to a uniform still water state.

The geometry of the channel together with the discretization of the physical domain are shown in Figure 3. A Manning coefficient for roughness was used with value $n = 0.03$. The discretization of the friction term was done semi-implicit with $\theta = 0.5$ due to the small value of the Manning coefficient. The solution was not sensitive to the change of the value of θ because the dominant term was the geometry not the friction. A triangular unstructured mesh with 1395 cells was used for the computation. Upstream and downstream boundaries are solid walls, CFL $= 0.9$.

Water depth contours are shown in Figure 4 together with velocity vectors at time: 0, 1, 2, 4, 20 and 120 s. The last one corresponds to steady-state. If no WDC or the one for steady flow were used in the computations the numerical calculation produced negative depths that were set to zero automatically. This generates mass error in both cases. Using the steady WDC the mass error is smaller but different from zero (1%) and if no WDC is applied mass error grows in time tending to large values. In Figure 5 time evolution of mass error is shown and proving that using the unsteady WDC together with negative depth control, error is zero

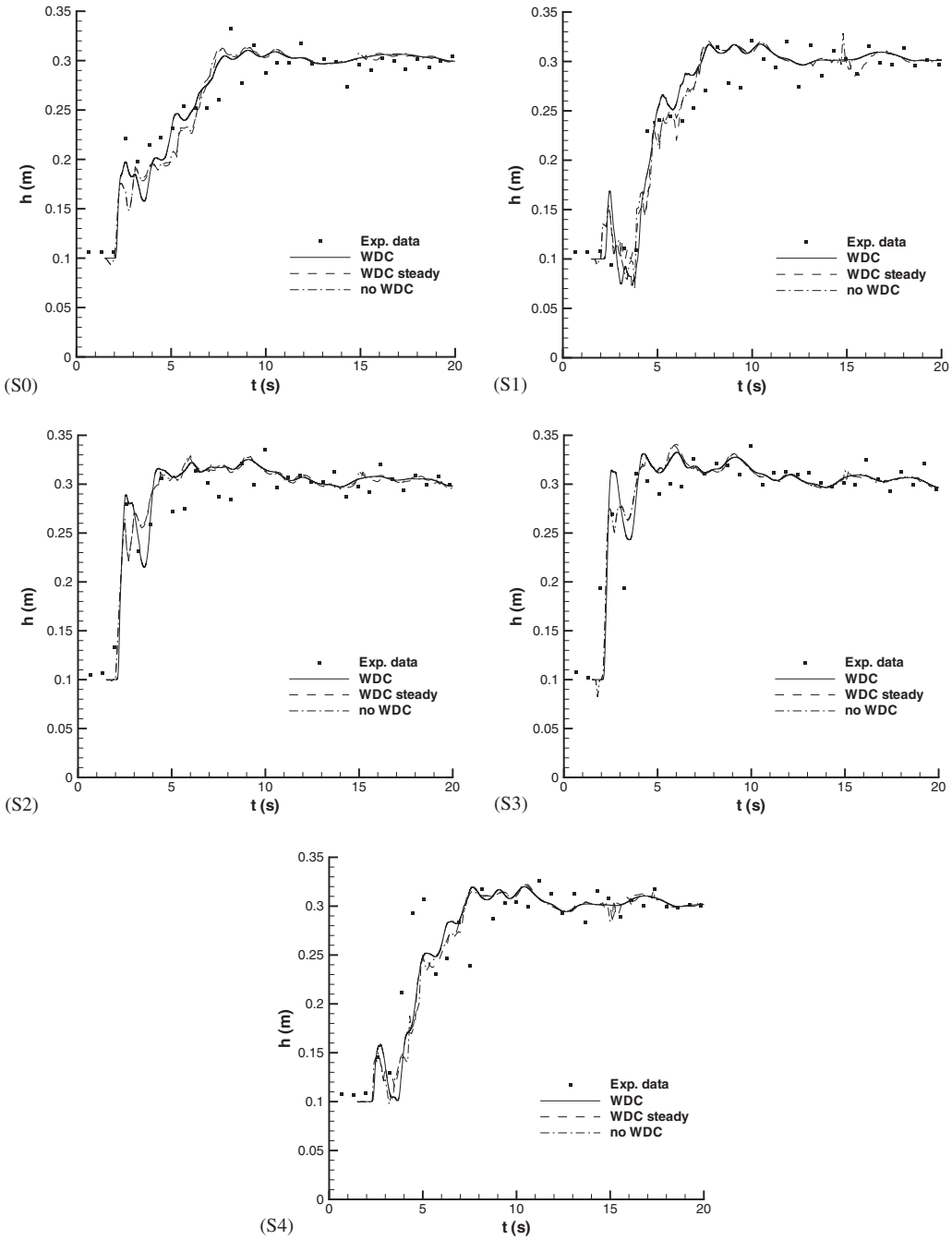

Figure 8. Experimental data and numerical results on the time evolution of water depth during 20 s at the measuring points S0, S1, S2, S3 and S4 located in Figure 7 in the simulation of a non-symmetric dam break in a pool with a pyramidal obstacle.

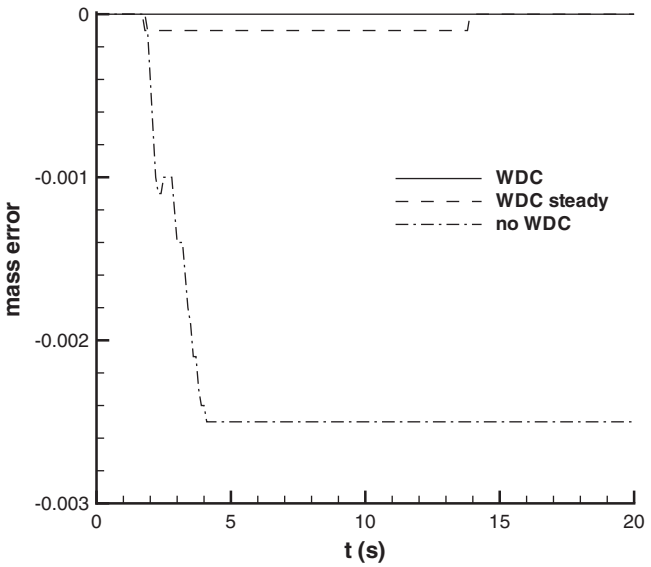

Figure 9. Time evolution during 20 s of mass error (m^3) using the unsteady WDC or the steady WDC or none in the simulation of a non-symmetric dam break in a pool with a pyramidal obstacle.

all the time. Mass error is computed as the difference between the initial volume of water and the volume of water computed after each time step ($V_{t^n} - V_{t^n+\Delta t}$) because there is no inflow or outflow contributions. When using WDC together with no negative depth control, the mass errors appear at $t = 0$ s when the rarefaction wave is formed after the dam break and they increase at around $t = 2$ s because the unsteady flow propagates towards the dry bank being it more dominant at that time. It can be seen in Figure 4 looking at the velocity vector profile at $t = 2$ s. At around $t = 2.3$ s it stays almost constant suggesting that there is no additional mass to the system because there is no relevant process of banks drying. All the computations carried out simulating subcritical flow, not only this example, give good results when using the unsteady WDC presented here. As we do not have any test with analytical solution to compare with, a simulation of the same test case has been carried out with CFL = 0.1 and the results at $t = 1, 2, 4$ and 20 s are shown in Figure 6 demonstrating that the solution obtained is the same.

7. NON-SYMMETRIC DAM BREAK IN A POOL WITH A PYRAMIDAL OBSTACLE

The physical model was built at the Hydraulic Lab. of CITEEC (Spain) under the supervision of J. Puertas. The model consists of a closed pool separated in two parts by a solid wall where a gate (dam) is located in a non-symmetric place (Figure 7). Details of the test can be found in Brufau *et al.* [18].

The experimental–numerical comparison corresponds to 0.5/0.1 m initial conditions. In Figure 8 experimental data and numerical results are compared on the time evolution of water depth during 20 s at the gauging points: S0, S1, S2, S3 and S4 around the pyramidal obstacle to check the wetting/drying condition WDC described here, the steady WDC and no

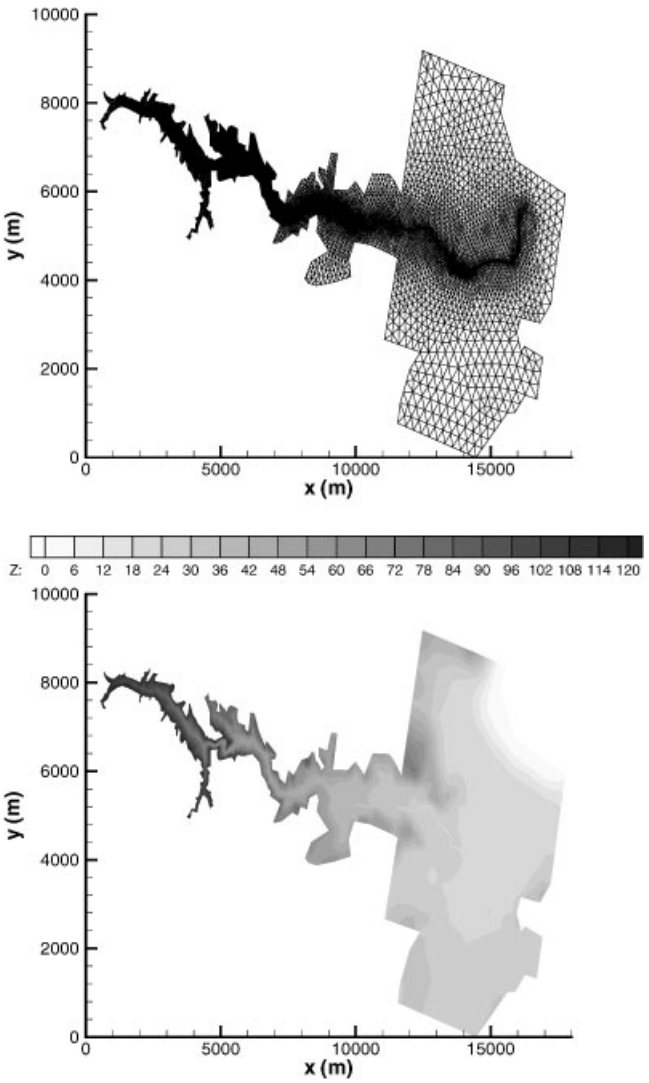

Figure 10. Unstructured mesh used in the computation and topography of the valley in the Malpasset dam failure.

use of WDC. A comparison of the time evolution of mass error using the WDC proposed here and the one used in Brufau *et al.* [18] for steady cases is shown in Figure 9.

8. MALPASSET DAM FAILURE

In 1959 the Malpasset arc dam near Frejus (France) broke almost instantaneously releasing an amount of about 48 million m^3 of water and caused 421 casualties [27, 28]. The real

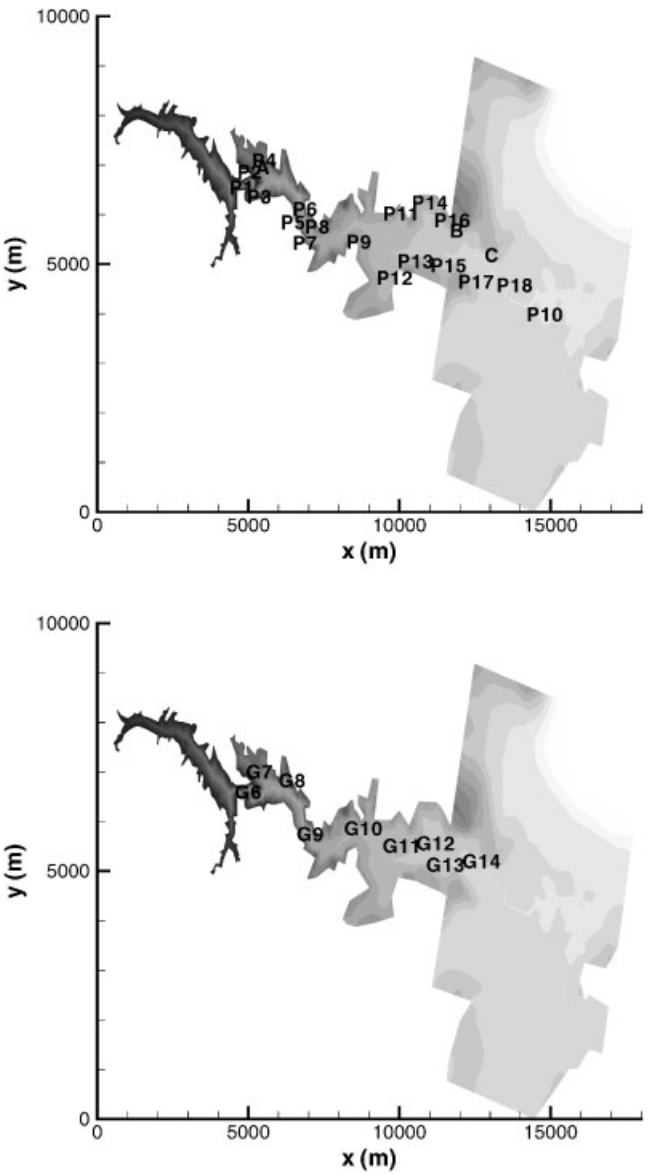

Figure 11. Location of the police (top) and physical model gauge points and transformers (bottom) on the Malpasset valley.

topography of the valley is shown in Figure 10. The reservoir is located on the left and the dam is at the end of the reservoir. On the first reach, the valley is rather sunken with two narrow bends. On the second reach it widens as some rivers and tributaries join the river. Further downstream it becomes narrow again before large bends and eventually reaching

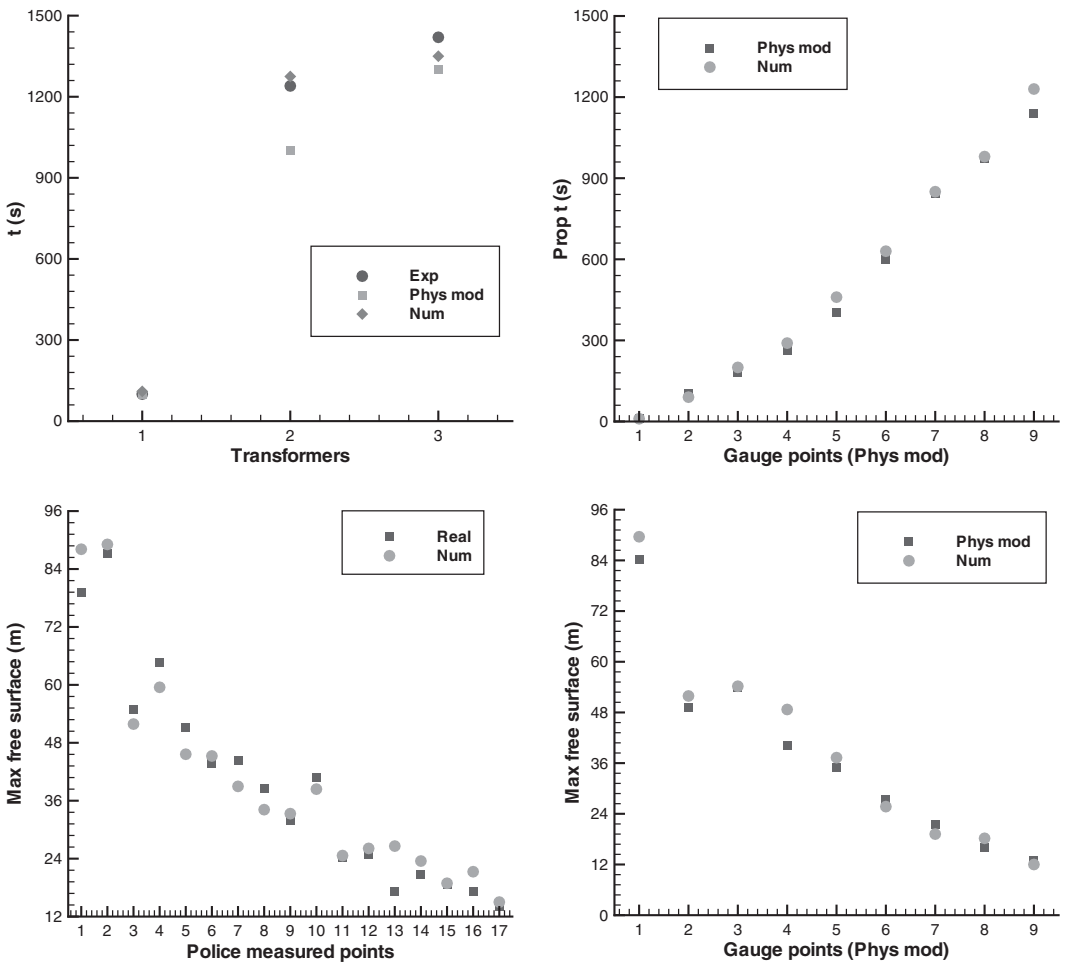

Figure 12. Comparison of numerical results with real data and physical model experiments can be observed.

a flat plain and finally it ends at the sea. The overall dimensions of the study reach are 17 500 m $\times$ 9000 m. This study was proposed by EDF in the frame of a European project (CADAM).

The police (gauge points labelled with P) collected detailed observations of the flood wave propagation and its maximum elevations on the right and left banks of the valley. Three transformers (A, B and C) were destroyed by the wave and the exact time of these shutdowns is known. In 1964 a $\frac{1}{400}$ physical model was constructed at EDF-LNH (Chatou) in order to get a better understanding of the flooding process (gauge points labelled with G at the centre of the valley). The maximum free surface elevation at these gauges was measured and is in good agreement with the observed high water marks [27].

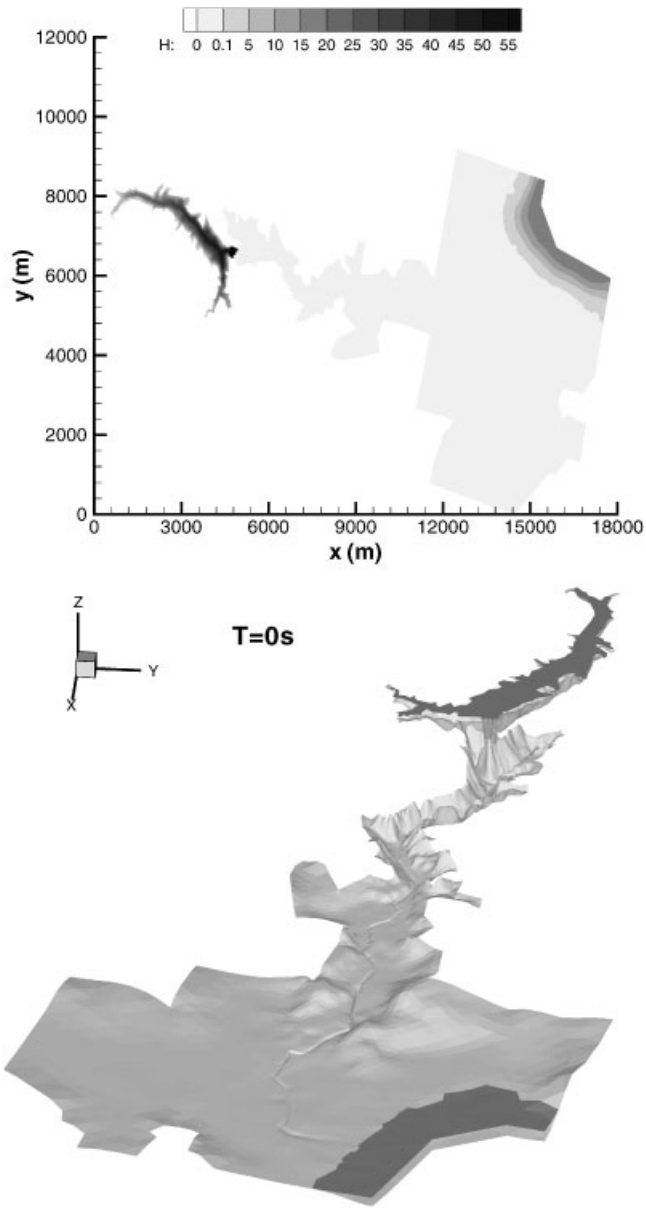

Figure 13. Contour water depths, velocity vectors and free surface at time: $t = 0, 1, 3, 13, 25$ and 33 min.

An unstructured triangular mesh has been used with 26 000 cells (Figure 10) and the time step is limited by CFL = 0.9. Manning coefficient for friction is 0.033. The parameter used for friction discretization is $\theta = 0.5$. The only open boundary is the sea with constant water level (0 m). Therefore, boundary conditions are free flow. For the initial conditions, water level is considered equal to 100 m in the reservoir and dry bed (0 m) in the river valley.

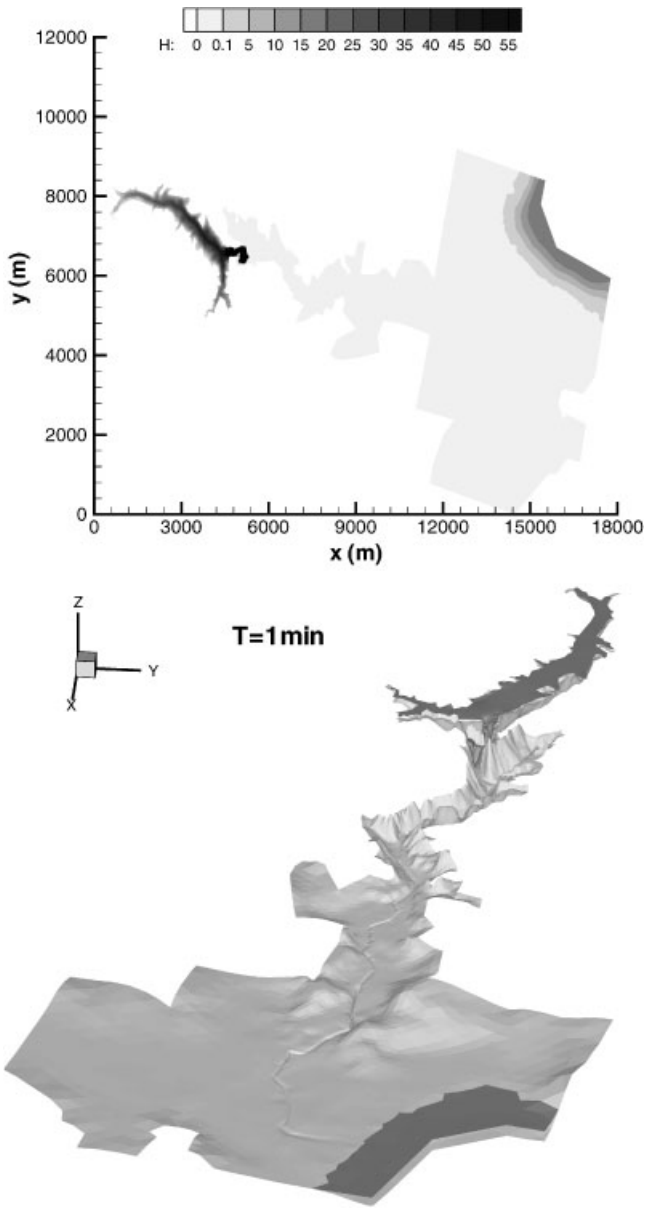

Figure 13. *Continued.*

Figure 11 shows the physical domain used for the numerical simulation where the gauge points (police and physical model) and transformers are located. The bed level is represented in the same figure with a contour plot. Comparison of numerical results with real data and physical model experiments can be observed referred to the arrival time to the transformers, arrival time to the gauge points at the physical model and maximum water level in terms of

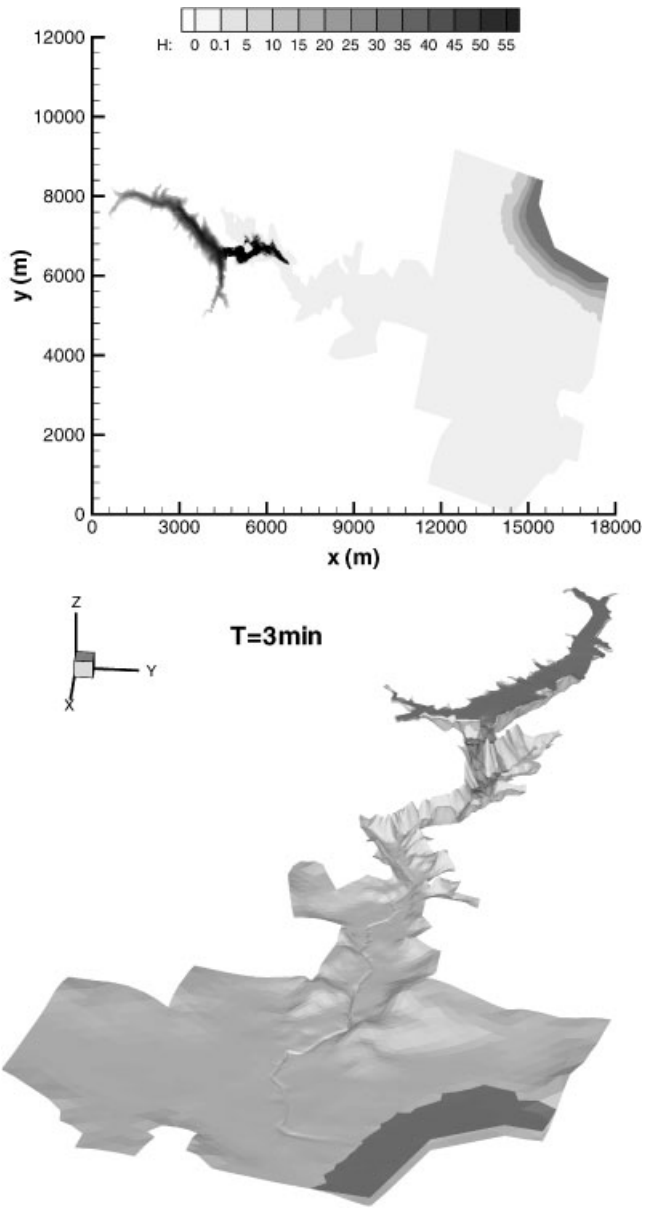

Figure 13. *Continued.*

free surface level at the physical model gauge points (Figure 12). Since transformer A was in the bottom of the valley, the shutdown here is the wave arrival time. For the other two transformers (B and C) the shutdown time is probably somewhere between the wave arrival time and the time of peak water level. Comparison of the maximum water level at the points

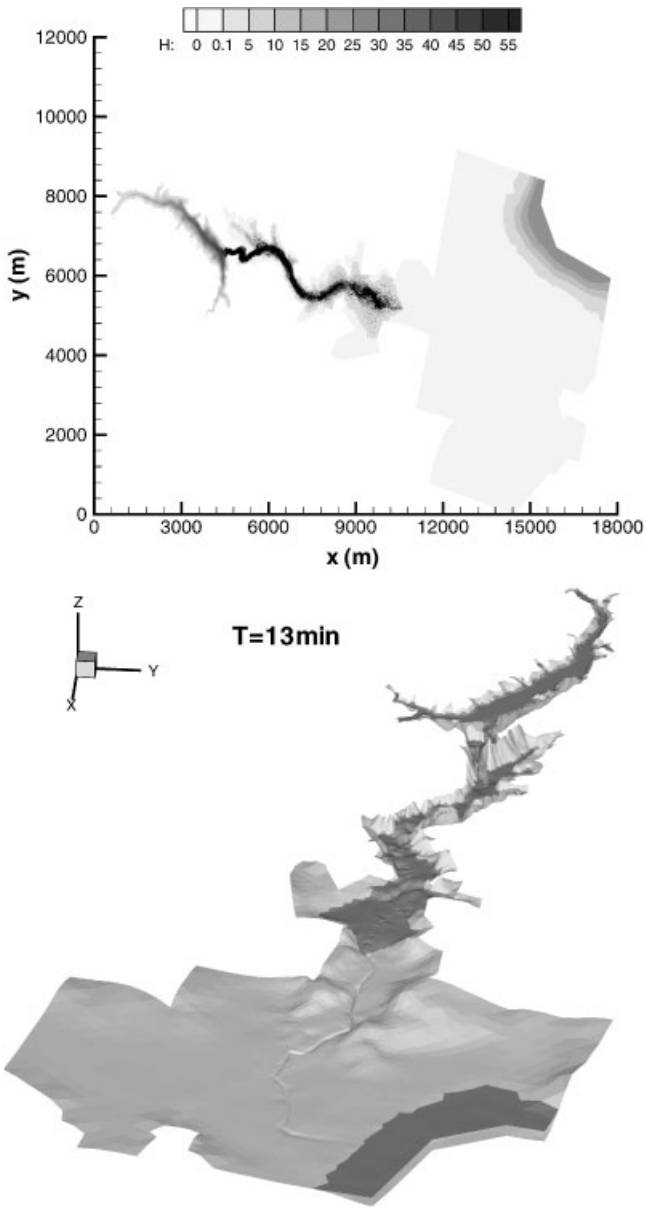

Figure 13. *Continued.*

measured by the police with the numerical results is shown in Figure 12. Snapshots at initial time ($t = 0$ s), $t = 3$, 13, 25 and 33 min of the free surface over the real topography of the valley are shown in Figure 13. Figure 14 represents the time evolution of the mass error in different situations. Mass error has been computed as the difference between the initial volume

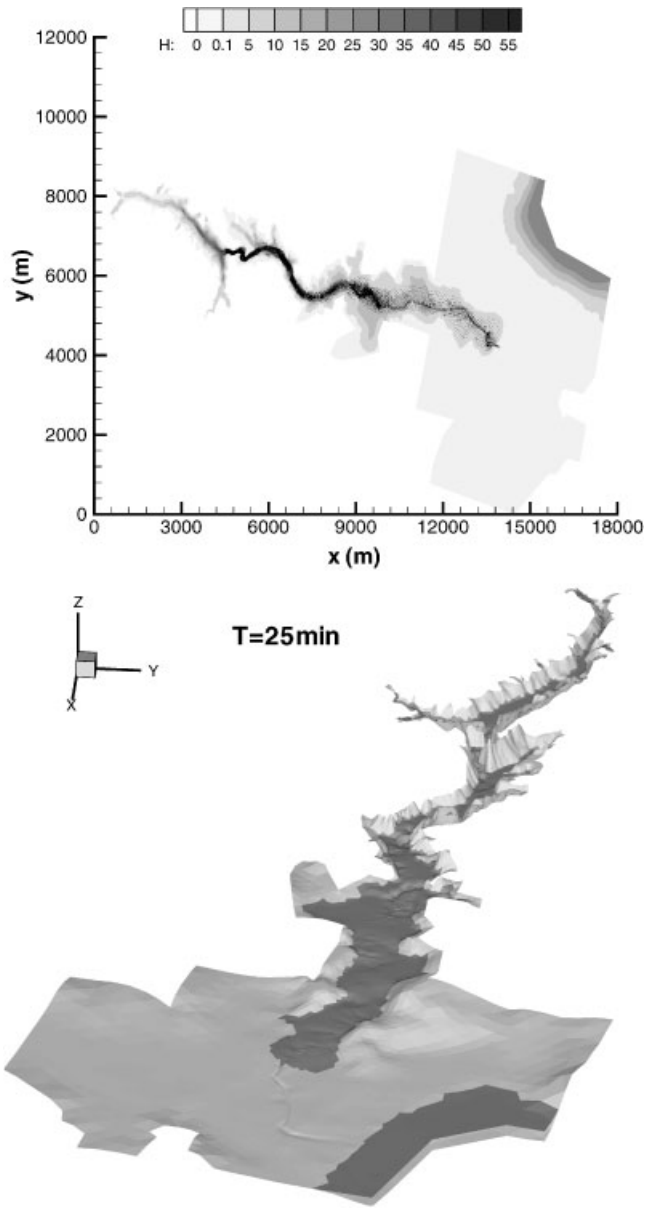

Figure 13. *Continued.*

of water and the one obtained after the computation was finished. In the figures, mass loses when there is no control of negative depths (see Section 4) can be appreciated. The use or not of the WDC does not make any difference in the mass error, which remains zero in both cases. This is because of the supercritical character of the flow and the WDC is mainly not applied in this case.

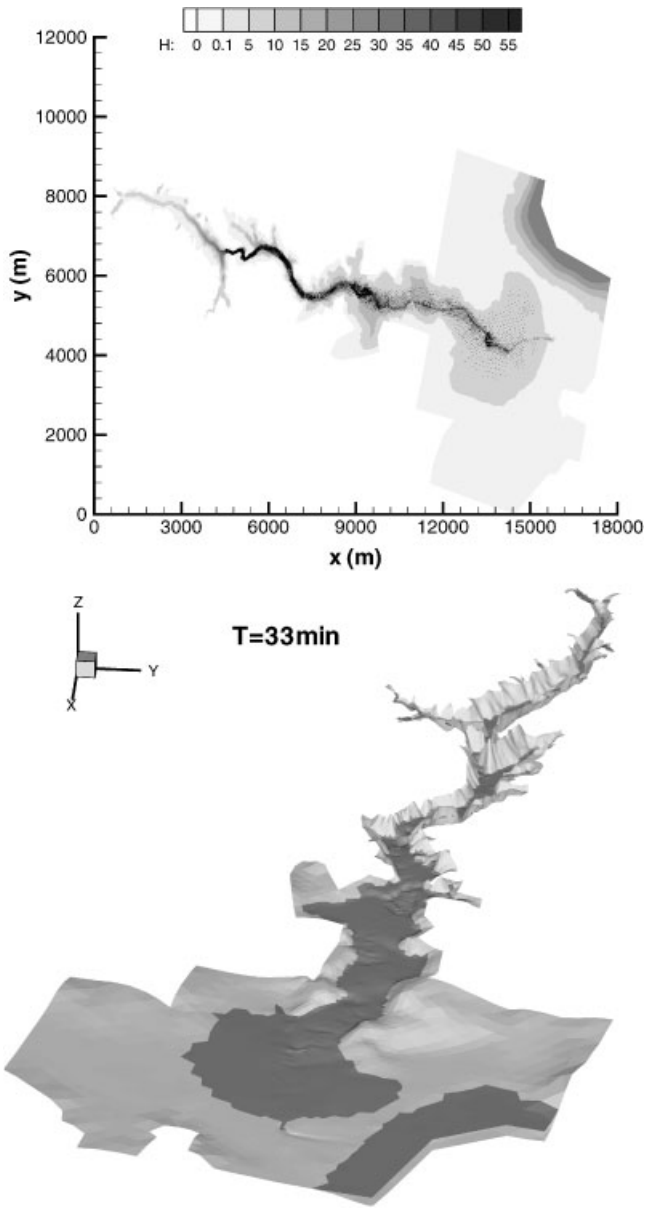

Figure 13. *Continued.*

Now, in Figures 15 and 16 we are going to analyse what happens with the water depth at the measured points (transformers, gauge and police) using or not the WDC and using or not the control of water depths. We can observe from the figures that in case the WDC is not used but the negative depths are controlled, corresponding to zero mass loses, there are small differences in water depth and time of arrival of the wave front to the transformers,

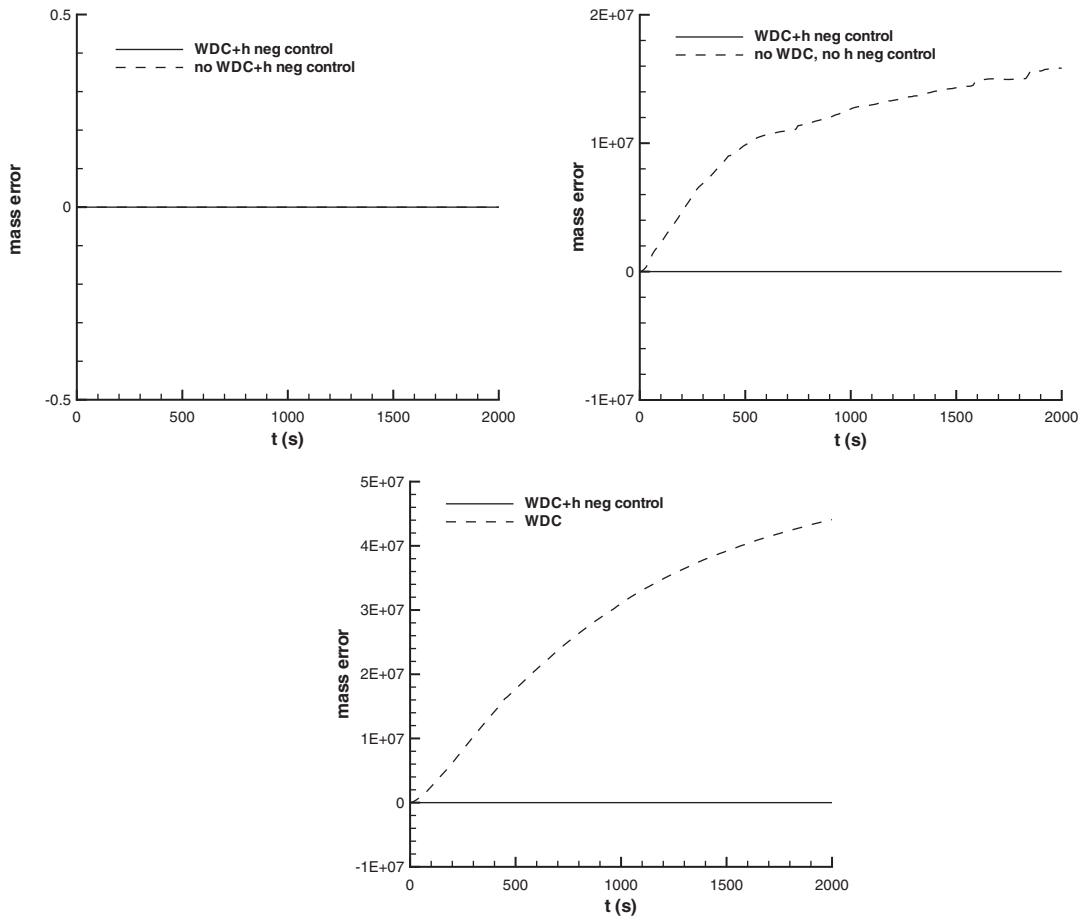

Figure 14. Time evolution of mass error (m^3) in the computation using or not the WDC and controlling or not negative depths.

police and gauge points (Figure 15). As expected, the differences are significant in the banks (police points) but meaningless in the centre of the river (gauge points). Only comparisons in a few upstream points are presented. In case the WDC is used but there is no control over the negative water depths which corresponds to a great amount of mass loses, comparison between time evolution of water depths in several points can be observed in Figure 16. As seen in Figure 14 a great amount of volume of water is lost in the computation when the negative depths are not controlled so there is no water depth in the transformers gauge or police points. The mass error has been computed as in the other test case.

9. CONCLUSIONS

An explicit finite volume upwind scheme has been used to solve the 2D shallow water system of equations. This numerical technique has been applied to the simulation of a flood wave

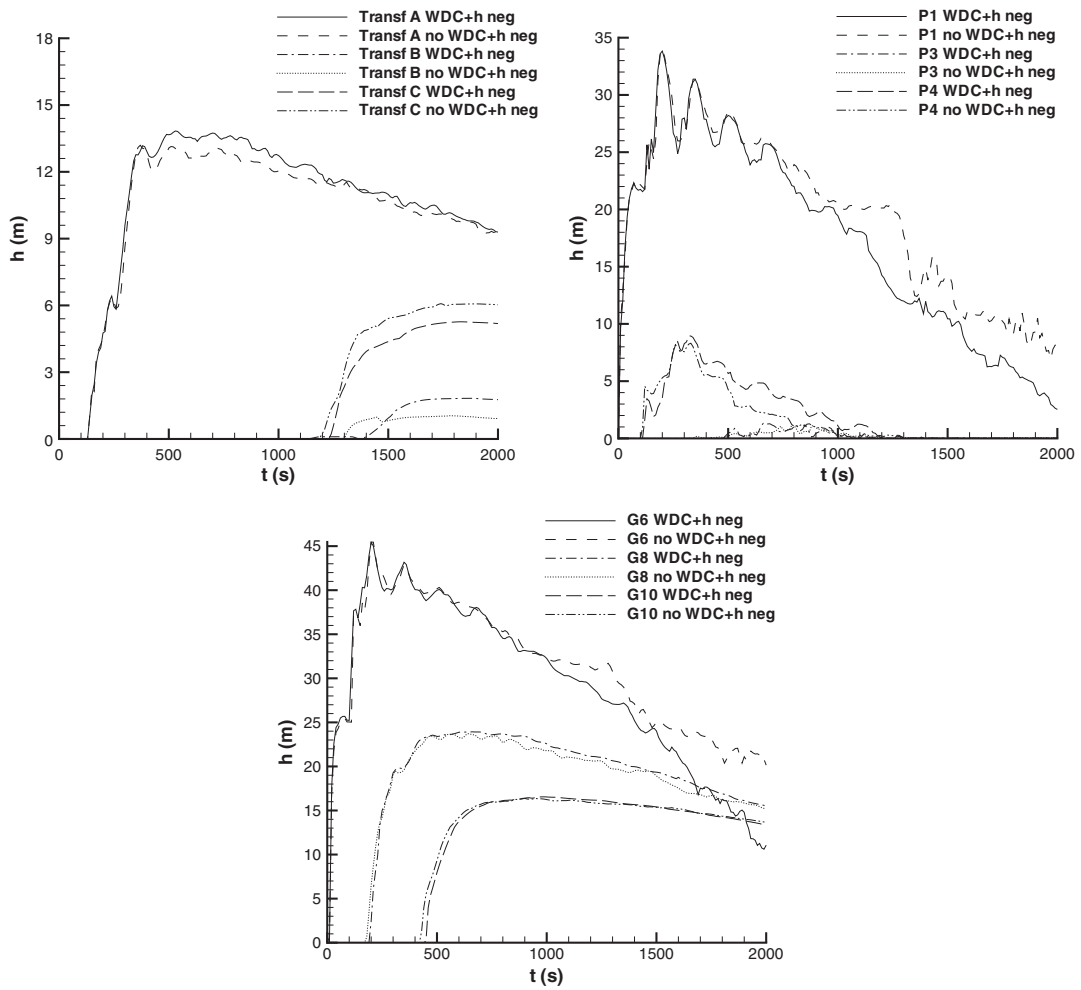

Figure 15. Comparison of numerical results using or not the WDC and controlling negative water depths in the transformers, police and gauge points.

produced by the Malpasset dam break in France. Source terms (bed variations and friction) are determinant in the solution of flows in complex geometries. There is an extra numerical work in the representation of the advancing and recessing front over inclined bed. The results have demonstrated the capability of the numerical scheme to simulate this kind of problems involving unsteady flows in complex geometries and solving appropriately the arrival time of the advancing front as well as the water depth levels. It can be observed that the initial volume of water has been conserved along the computation. Upwinding bed slope terms and wetting–drying condition for unsteady flow combined with the classical upwind scheme for fluxes give a fully conservative numerical technique without numerical errors. The wetting–drying condition for unsteady flow gives zero mass error which demonstrates the effectiveness

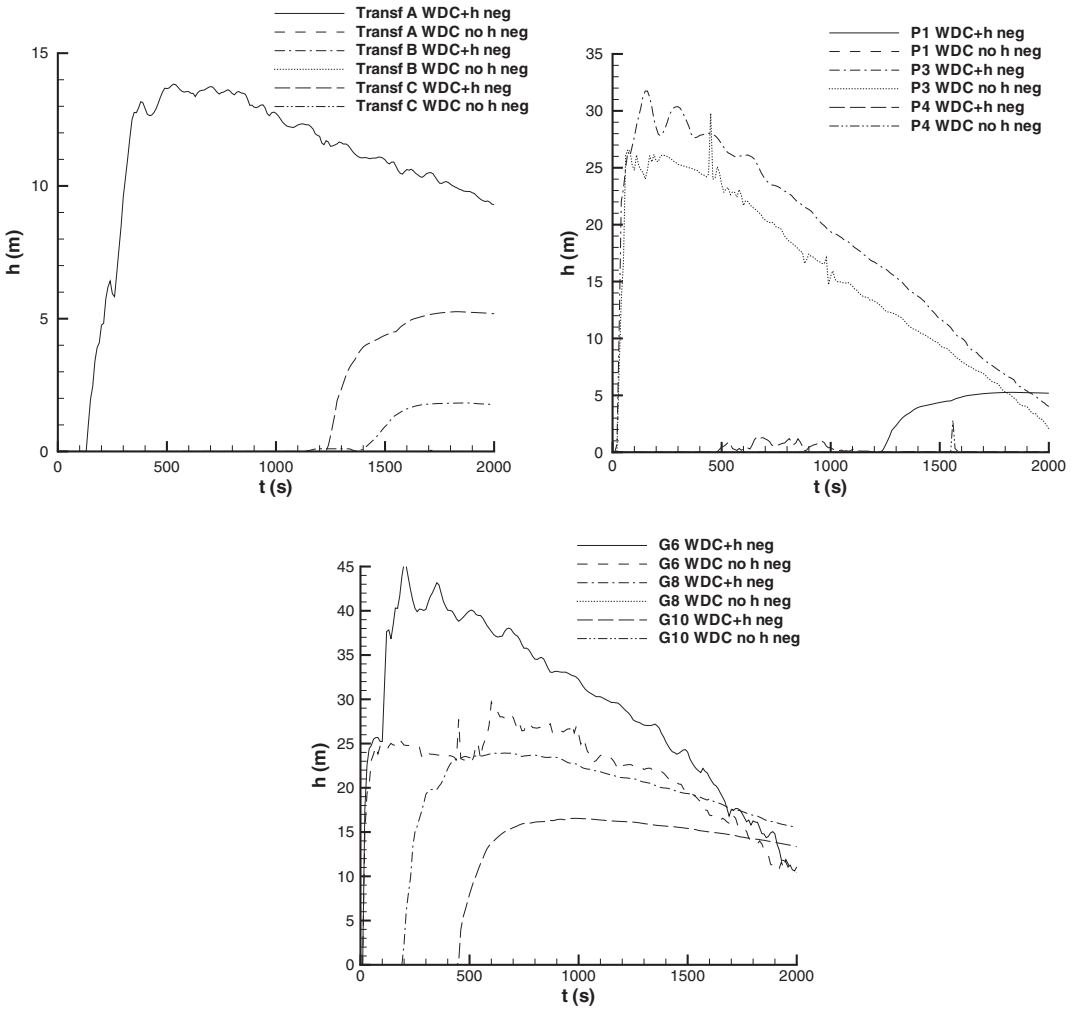

Figure 16. Comparison of numerical results using the WDC and controlling or not negative water depths in the transformers, police and gauge points.

of the numerical scheme to simulate real events. Numerical techniques developed in the last decade to solve realistic problems do not always take in care source terms discretization or the treatment of wetting–drying fronts. This work completes a well-known numerical technique conserving the total amount of water which is a quality control of the numerical solution of maximum interest in Hydraulic Engineering.

ACKNOWLEDGEMENTS

The authors would like to thank the data supplied by N. Goutal (EDF-LNH Chatou) under the European concerted action project on dam break modelling (CADAM) and CITEEC (Spain) for providing experimental data for this research.

REFERENCES

1. Abbott MB. *Computational Hydraulics*. Ashgate Publishing Company: New York, USA, 1992.
2. Cunge JA, Holly FM, Verwey A. *Practical Aspects of Computational River Hydraulics*. Pitman: London, UK, 1980.
3. Sleigh PA, Berzins M, Gaskell PH, Wright NG. An unstructured finite volume algorithm for predicting flow in rivers and estuaries. *Computers and Fluids* 1998; **27**(4):479–508.
4. García-Navarro P, Fras A, Villanueva I. Dam break flow simulation: some results for one dimensional models of real cases. *Journal of Hydrology* 1999; **216**:227–247.
5. Zhao DH, Shen HW, Tabios GQ, Lai JS, Tan WY. Finite volume two-dimensional unsteady flow model for river basins. *Journal of Hydraulic Engineering* 1994; **120**(7):863–883.
6. Bermúdez A, Vázquez ME. Upwind methods for hyperbolic conservation laws with source terms. *Computers and Fluids* 1994; **8**:1049–1071.
7. Vázquez-Cendón ME. Improved treatment of source terms in upwind schemes for the shallow water equations in channels with irregular geometry. *Journal of Computational Physics* 1999; **148**:497–526.
8. Akanbi AA, Katopodes ND. Model for flood propagation on initially dry land. *Journal of Hydraulic Engineering*—ASCE 1987; **114**(7):689–706.
9. Meselhe EA, Holly FM. Simulation of unsteady flow in irrigation canals with a dry bed. *Journal of Hydraulic Engineering*—ASCE 1993; **119**:1021–1030.
10. Tchamen GW, Kahawita R. The numerical simulation of wetting and drying areas using Riemann solvers. *Proceedings of Modeling of Flood Propagation over Initially Dry Areas*, Milan, Italy, 1994.
11. Kramer T, Jozsa J, Sarkkula J. Hydrodynamic modeling aspects in the restoration planning of a coastal wetland. *Proceedings of the XXIX IAHR Congress*, Beijing, 2001.
12. Beffa C, Connel R. Two-dimensional flood plain flow. I: model description. *Journal of Hydraulic Engineering*—ASCE 2001; **6**(5):397–405.
13. George KJ, Stripling S. Improving the simulation of drying and wetting in a two-dimensional tidal numerical model. *Applied Mathematical Modeling* 1995; **19**(1):2–6.
14. Heniche M, Secretan Y, Boudreau P, Leclerc M. A two-dimensional finite element drying–wetting shallow water model for rivers and estuaries. *Advances in Water Resources*, Elsevier Science, 2000; **23**:359–372.
15. Kawahara M, Umetsu T. Finite element method for moving boundary problems in river flow. *International Journal for Numerical Methods in Fluids* 1986; **6**:365–386.
16. Khan AA. Modeling flow over an initially dry bed. *Journal of Hydraulic Research* 2000; **38**(5):383–389.
17. Bradford SF, Sanders BF. Finite-volume model for shallow water flooding of arbitrary topography. *Journal of Hydraulic Engineering* 2002; **128**(3):289–298.
18. Brufau P, Vázquez-Cendón ME, García-Navarro P. A numerical model for the flooding and drying of irregular domains. *International Journal for Numerical Methods in Fluids* 2002; **39**:247–275.
19. Chow VT. *Open Channel Hydraulics*. MacGraw-Hill Book Company Incorporation: New York, 1959.
20. LeVeque RJ. Balancing source terms and flux gradients in high-resolution Godunov methods: the quasi-steady wave-propagation algorithm. *Journal of Computational Physics* 1998; **146**(1):346–365.
21. Bermúdez A, Dervieux A, Desideri JA, Vázquez ME. Upwind schemes for the two-dimensional shallow water equations with variable depth using unstructured meshes. *Computer Methods in Applied Mechanics and Engineering* 1998; **155**:49–72.
22. García-Navarro P, Vázquez-Cendón ME. On numerical treatment of the source terms in the shallow water equations. *Computers and Fluids* 2000; **29**:951–979.
23. Hubbard ME, García-Navarro P. Flux difference splitting and the balancing of source terms and flux gradients. *Journal of Computational Physics* 2000; **165**:89–125.
24. Roe PL. *A Basis for Upwind Differencing of the Two-Dimensional Unsteady Euler Equations*. Numerical Methods in Fluid Dynamics, vol. II. Oxford University Press: Oxford, 1986.
25. Brufau P, García-Navarro P. Two-dimensional dam break flow simulation. *International Journal for Numerical Methods in Fluids* 2000; **33**:35–57.
26. Hirsch C. *Numerical Computation of Internal and External Flows*, vol. 2. Wiley: New York, 1990.
27. Goutal N. The Malpasset dam failure. An overview and test case definition. *Proceedings of Zaragoza Meeting*, *CADAM Project*, 1999.
28. Hervouet JM, Petitjean A. Malpasset dam-break revisited with two-dimensional computations. *Journal of Hydraulic Research* 1999; **37**:777–788.
29. Bento Franco A. *Modelacao computacional e experimental de escoamentos provocados por roturas de barragens*. Ph.D. Dissertation, University Técnica de Lisboa, 1996.

